Monthly Notices
of the
ROYAL ASTRONOMICAL SOCIETY

MNRAS **448,** 237–251 (2015) doi:10.1093/mnras/stu2755

Two conditions for galaxy quenching: compact centres and massive haloes

Joanna Woo,[1,2]★ Avishai Dekel,[2] S. M. Faber[3] and David C. Koo[3]

[1]*Institute for Astrophysics, Department of Physics, ETH Zurich, Wolfgang-Pauli-Strasse 27, CH-8093 Zurich, Switzerland*
[2]*Center for Astrophysics and Planetary Science, Racah Institute of Physics, The Hebrew University, Jerusalem 91904, Israel*
[3]*University of California Observatoires/Lick Observatory, Department of Astronomy and Astrophysics, University of California, Santa Cruz, CA 95064, USA*

Accepted 2014 December 30. Received 2014 December 3; in original form 2014 June 19

ABSTRACT

We investigate the roles of two classes of quenching mechanisms for central and satellite galaxies in the Sloan Digital Sky Survey ($z < 0.075$): those involving the halo and those involving the formation of a compact centre. For central galaxies with inner compactness $\Sigma_{1\,\mathrm{kpc}} \sim 10^{9\text{–}9.4}\,\mathrm{M_\odot\,kpc^{-2}}$, the quenched fraction f_q is strongly correlated with $\Sigma_{1\,\mathrm{kpc}}$ with only weak halo mass M_h dependence. However, at higher and lower $\Sigma_{1\,\mathrm{kpc}}$, specific star formation rate (sSFR) is a strong function of M_h and mostly independent of $\Sigma_{1\,\mathrm{kpc}}$. In other words, $\Sigma_{1\,\mathrm{kpc}} \sim 10^{9\text{–}9.4}\,\mathrm{M_\odot\,kpc^{-2}}$ divides galaxies into those with high sSFR below and low sSFR above this range. In both the upper and lower regimes, increasing M_h shifts the entire sSFR distribution to lower sSFR without a qualitative change in shape. This is true even at fixed M_*, but varying M_* at fixed M_h adds no quenching information. Most of the quenched centrals with $M_\mathrm{h} > 10^{11.8}\,\mathrm{M_\odot}$ are dense ($\Sigma_{1\,\mathrm{kpc}} > 10^{9}\,\mathrm{M_\odot\,kpc^{-2}}$), suggesting compaction-related quenching maintained by halo-related quenching. However, 21 per cent are diffuse, indicating only halo quenching. For satellite galaxies in the outskirts of haloes, quenching is a strong function of compactness and a weak function of host M_h. In the inner halo, M_h dominates quenching, with ∼90 per cent of the satellites being quenched once $M_\mathrm{h} > 10^{13}\,\mathrm{M_\odot}$. This regional effect is greatest for the least massive satellites. As demonstrated via semi-analytic modelling with simple prescriptions for quenching, the observed correlations can be explained if quenching due to central compactness is rapid while quenching due to halo mass is slow.

Key words: galaxies: evolution – galaxies: general – galaxies: groups: general – galaxies: haloes – galaxies: star formation – galaxies: structure.

1 INTRODUCTION

Large surveys of galaxies over the last decade have established that the nature of galaxies is bimodal. Their populations are effectively described as either blue and star forming or red and quiescent. The star-forming population tends to exhibit disc-like morphologies and low central densities, while the quiescent galaxies host a dominant bulge component with high central densities (Strateva et al. 2001; Blanton et al. 2003; Kauffmann et al. 2003a; Baldry et al. 2004; Wuyts et al. 2011; Cheung et al. 2012). While galaxies are expected to accrete gas and form stars, it is still a mystery how the quiescent population originated.

Several mechanisms have been proposed to explain the shut-down of star formation. Among them, the 'halo quenching' mechanism has been the major reason behind the success of galaxy formation models in reproducing several aspects of the bimodality (Bower et al. 2006; Croton et al. 2006; Cattaneo et al. 2008). Quenching in these models hinges upon a critical halo mass M_crit (a few $\times 10^{12}\,\mathrm{M_\odot}$), below which accretion is cold and conducive to star formation. Above M_crit, infalling gas reaches the sound speed and a stable shock forms. This shock heats the gas and prevents its accretion on to the central galaxy to form stars (Rees & Ostriker 1977; Birnboim & Dekel 2003; Kereš et al. 2005). For a population of haloes, this should not be interpreted as a sharp threshold but rather as a mass range extending over one or two decades where there is a decrease in the cold accretion as a function of halo mass (M_h; Ocvirk, Pichon & Teyssier 2008; Kereš et al. 2009; van de Voort et al. 2011).

While halo quenching successfully reproduces the bimodality of star formation when implemented as a strong, immediate effect, it does not naturally explain the link between quiescence and a prominent bulge, structural compactness or high central density. Among the proposed bulge-building/compacting quenching mechanisms is the major merger scenario, in which a central spheroid forms through the violent relaxation of pre-merger stars (Toomre & Toomre 1972; Mihos & Hernquist 1994; Hopkins et al. 2009). Furthermore, gas is driven to the central regions of the system,

★ E-mail: joanna.woo@phys.ethz.ch

producing a starburst that quickly exhausts the gas (through consumption and winds) and contributes to the central compactness. Active galactic nuclei (AGN) triggered in the merger also suppress star formation. However, it is uncertain whether major mergers actually quench galaxies (Coil et al. 2011), or whether the merger rate is sufficient to account for the number of bulges (Hopkins et al. 2010; Lotz et al. 2011).

Another process that builds a compact bulge is gaseous inflow through violent disc instability, including the migration of giant star-forming clumps (Noguchi 1999; Bournaud, Elmegreen & Elmegreen 2007; Dekel, Sari & Ceverino 2009; Dekel & Burkert 2014; Mandelker et al. 2014). Infalling cold streams maintain the unstable disc and replenish the gas. These gaseous inflows may fuel AGN and consume gas via high star formation rates and powerful outflows creating a central concentration of young stars in a dense 'blue nugget'. This process depends on a strong gas inflow rate, which occurs at $z \gtrsim 2$, but declines with time.

The build-up of the bulge through mergers or instabilities can stabilize the disc against further star formation (see also Martig et al. 2009). This can also be coupled with a mechanism that shuts off accretion, such as virial shock heating or AGN heating, which cuts the supply of the gas that fuels both star formation and disc instabilities.

As for satellite galaxies, the above mechanisms may have operated on these while they were still centrals. However, there are additional quenching mechanisms that are unique to satellites such as strangulation (the cut-off cold accretion; Larson, Tinsley & Caldwell 1980; Balogh, Navarro & Morris 2000), ram pressure stripping (the stripping of both cold and hot gas due to movement through a hot medium; Gunn & Gott 1972; Abadi, Moore & Bower 1999), tidal stripping (the stripping of gas and stars outside the tidal radius as a satellite approaches pericentre; Read et al. 2006) and harassment (heating of cold gas due to high-speed satellite–satellite interactions; Moore, Lake & Katz 1998; Villalobos et al. 2012). These mechanisms are expected to be more efficient near the centres of haloes.

Several studies have attempted to observationally constrain or rule out any of these scenarios with conflicting results. For example, quenching for central galaxies is observed to correlate more strongly with an estimate of halo mass $M_{\rm h}$ than with luminosity (Weinmann et al. 2006) or stellar mass M_* (Woo et al. 2013), supporting the halo quenching scenario (see also Tal et al. 2014). Halo quenching is also consistent with the many studies that find a dependence of quenching on environment and clustering (Hogg et al. 2003; Balogh et al. 2004; Kauffmann et al. 2004; Blanton et al. 2005a; Baldry et al. 2006; Bundy et al. 2006; Cooper et al. 2008; Skibba & Sheth 2009; Wilman, Zibetti & Budavári 2010; Haas, Schaye & Jeeson-Daniel 2012; Quadri et al. 2012; Hartley et al. 2013). However, quenching also has a strong dependence on morphology and galaxy structure in the local Universe (Kauffmann et al. 2003b; Bell 2008; Franx et al. 2008; van Dokkum et al. 2011; Robaina et al. 2012; Bluck et al. 2014; Omand, Balogh & Poggianti 2014) and at high-z (Wuyts et al. 2011, 2012; Bell et al. 2012; Cheung et al. 2012; Szomoru, Franx & van Dokkum 2012; Barro et al. 2013; Lang et al. 2014), which is not expected in halo quenching, but in bulge-building mechanisms. Furthermore, galaxies which may be transitioning from star formation to quiescence appear to have early-type morphologies (Mendel et al. 2013). On the other hand, while bulge-building mechanisms succeed in producing compact inner regions, they do not address the observed quenching of disc galaxies which may represent 25–65 per cent of quenched galaxies, especially at high-z (Stockton, Canalizo & Maihara 2004; McGrath et al. 2008; van Dokkum et al. 2008; van den Bergh 2009; Bundy et al. 2010; van der Wel et al. 2011; Bruce et al. 2012; Salim et al. 2012; Bruce et al., 2014). The quenching of such galaxies is more naturally explained as a halo process, whether as centrals (van den Bergh 2009; Bundy et al. 2010) or satellites (Peng et al. 2010, 2012; Bell et al. 2012; Knobel et al. 2013; Kovač et al. 2014). Thus it remains unclear how important the halo environment is compared to galaxy morphology/structure in predicting quenching.

For satellites, the quenching picture is not any clearer. Quenching has been observed to correlate with cluster-/groupcentric distance (Gómez et al. 2003; Balogh et al. 2004; Tanaka et al. 2004; Rines et al. 2005; Blanton & Roweis 2007; Haines et al. 2007; Hansen et al. 2009; Wolf et al. 2009; von der Linden et al. 2010; Woo et al. 2013) supporting the various satellite quenching scenarios that operate in dense environments. The quenching of satellites also seems to depend on environment more than morphology (Koopmann & Kenney 1998; Goto et al. 2003; Kodama et al. 2004; Vogt et al. 2004; Bamford et al. 2009; Wolf et al. 2009). This can naturally be explained by the presence of hot gas in massive haloes (Gabor & Davé 2014), which is conducive to, for instance, ram pressure stripping. However, others have argued that colours and red fractions of satellites are determined by a galaxy's stellar mass M_* (van den Bosch et al. 2008; Peng et al. 2010, 2012) and number density of surrounding galaxies (Peng et al. 2010, 2012) rather than by an estimate of its host halo mass $M_{\rm h}$. Woo et al. (2013), on the other hand, showed that the importance of a satellite's M_* versus its host $M_{\rm h}$ in predicting quenching depends on where the satellite lies in its halo. This could reflect residual 'central' quenching before infall, coupled with a 'delayed-then-rapid' form of satellite quenching (Mok et al. 2013; Trinh et al. 2013; Wetzel et al. 2013). Omand et al. (2014) recently showed that satellite structure rather than M_* determines satellite quenching, but Carollo et al. (2014) showed that the fraction of morphologically early-type satellites is independent of environment. Some of these confusions can be resolved by comparing the importance of bulge-related processes on satellites to halo-related processes at different groupcentric radii.

The goal of this paper is to study the effectiveness of halo-related and bulge/compactness-related quenching in centrals and satellites in the Sloan Digital Sky Survey (SDSS).

'Compactness-related' quenching (also related to the bulge) will be measured by the central surface density within the inner 1 kpc ($\Sigma_{1\,\rm kpc}$) following Cheung et al. (2012) and Fang et al. (2013) since this quantity probes quenching mechanisms that involve gaseous inflows towards a galaxy's central regions. Additionally, Cheung et al. (2012) and Fang et al. (2013) showed that $\Sigma_{1\,\rm kpc}$ is a stronger predictor for quenching than the bulge-to-total ratio B/T and Sérsic n.

'Halo-related' quenching for centrals can in principle be explored using direct estimates of $M_{\rm h}$ or using M_* as a proxy since the two are tightly related for centrals. In fact, Fang et al. (2013) showed that the combination of the inner compactness and stellar mass M_* strongly predicts quenching for central galaxies. Since Woo et al. (2013) showed that $M_{\rm h}$ predicts quenching for centrals better than M_*, this motivates a similar analysis with $M_{\rm h}$ instead of M_*. Moreover, $M_{\rm h}$ provides some advantages over M_*. First, M_* confuses the relation between internal and external quenching mechanisms since it is an internal property which tightly correlates with the inner compactness, as well as with $M_{\rm h}$ for centrals. Thus, it is unclear whether correlations of quenching with M_* point to halo-related quenching or to internal quenching processes. Second, as described above, there are quenching mechanisms that are directly related to the halo and to the inner compactness, but there are no known mechanisms

for quenching that are directly related to the stellar mass for massive galaxies. The net result of this analysis will validate the use of $M_{\rm h}$ over M_* for centrals as expected theoretically. Lastly, M_* satellites is largely unrelated to host $M_{\rm h}$ and any associated halo processes.

Quenching will be measured using the quenched fraction $f_{\rm q}$ of galaxies along with the specific star formation rate (sSFR) = star formation rate (SFR)/M_*. These are defined in Section 2 along with all data used in this study. Our results for centrals will be presented in Section 3 and satellites in Section 4. Section 5 will discuss an interpretation of our findings as a result of slow and rapid quenching, with concluding remarks in Section 6.

This analysis assumes concordance cosmology: $H_0 = 70\,{\rm km\,s^{-1}\,Mpc^{-1}}$, $\Omega_{\rm M} = 0.3$, $\Omega_\Lambda = 0.7$. Halo masses are converted to this cosmology with $\sigma_8 = 0.9, \Omega_{\rm b} = 0.04$.

Our conclusions from this analysis will be that both halo-related and compactness-related quenching govern the evolution of centrals and satellites in such a way that may point to a difference in duration for the two types of quenching.

2 DATA

2.1 The sample

The SDSS (York et al. 2000, Gunn et al. 2006) sample used throughout this analysis is from the Data Release 7 (DR7 - Abazajian et al. 2009) limited to the redshift range $0.005 < z < 0.075$. This sample contains 65 939 galaxies after matching all catalogues and applying all cuts as described below.

Using the *K*-correction utilities of Blanton & Roweis (2007), v4_2, we calculate $V_{\rm max}$ from *ugriz* photometry ('petro' values - Gunn et al. 1998, Doi et al. 2010) and redshifts from the New York University Value-Added Galaxy Catalog (NYU-VAGC; DR7) catalogue (Blanton et al. 2005b; Adelman-McCarthy et al. 2008; Padmanabhan et al. 2008) and the *r*-band limit (17.77) of the spectroscopic survey. We weight each galaxy by its $1/V_{\rm max}$ multiplied by the inverse of its spectroscopic completeness (also obtained from the NYU-VAGC). All quoted galaxy fractions and volume densities are weighted.

The NYU-VAGC contains 2506 754 objects, of which 207 005 are classified as galaxies (SPECCLASS = 2), is a primary spectroscopic object (SPECPRIMARY = 1), is an object for which KCORRECT produced finite $V_{\rm max}$ and lies within our chosen redshift range.

2.2 Stellar masses

Stellar mass M_* is taken from the DR7 catalogue provided online by Brinchmann et al.[1] Using a Kroupa (2001) initial mass function (IMF), they derived M_* through spectral energy distribution (SED) fitting similar to the method that Salim et al. (2007) used for estimating SFRs, and the method used by Kauffmann et al. (2003a) to derive M_* by fitting spectral features rather than photometry. These stellar mass estimates differ from Kauffmann et al. (2003a) by less than 0.1 dex for $M_* \gtrsim 10^9\,{\rm M}_\odot$. The formal 1σ errors are typically about 0.05 dex or less (from the 95 per cent confidence intervals of the probability distribution).

This catalogue contains 927 552 objects, 198 159 of which match the NYU-VAGC and pass our cuts described above. Of these, 182 406 are above our cut of $M_* = 10^9\,{\rm M}_\odot$.

[1] http://www.mpa-garching.mpg.de/SDSS/DR7/

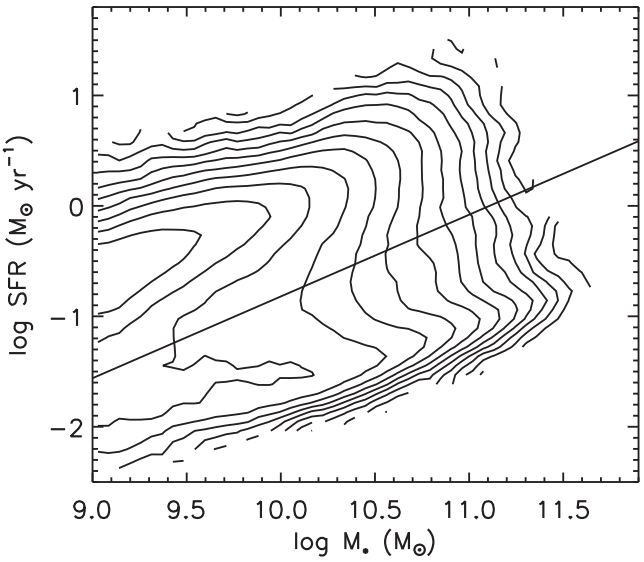

Figure 1. SFR versus M_* for our total galaxy sample. The solid line marks our division between star-forming and quenched galaxies.

2.3 SFR

Brinchmann et al. (2004) estimated SFR for the DR4, and those used here are an updated and improved version for the DR7. They are provided online by J. Brinchmann et al.[1] As in Brinchmann et al. (2004), these SFR estimates are calibrated to the Kroupa (2001) IMF, and combine measurements inside and outside the fibre. Inside the fibre, SFR is estimated from Hα and Hβ lines for star-forming galaxies. SFR for galaxies with weak lines or showing evidence for AGN is estimated using the relation between the D4000 break and Hα and Hβ lines observed in star-forming galaxies. Outside the fibre, they fit stellar population models to the observed photometry following the method of Salim et al. (2007). The means of the resulting probability distribution function of SFR were added to the SFR estimates in the fibre for an estimate of the total SFR. These SFR estimates account for dust in the SED modelling, and we have confirmed that applying a selection on inclination ($b/a > 0.5$) does not affect our results.

The original catalogue contains 927 552 objects, 182 406 of which pass our previous cuts. Of these, we select 182 125 that are flagged with SFFLAG = 0 (all other SFRs were measured with slightly different methods and could introduce bias).

The typical errors of these SFRs are estimated by Brinchmann (private communication) to be about 0.4 dex for star-forming galaxies, 0.7 dex for intermediate galaxies and 1 dex or more for dead galaxies. For the dead galaxies, the given SFR values should be considered as upper limits rather than measurements. However, a comparison of these SFR estimates with those of Salim et al. (2007), which are derived from SED fitting of ultraviolet (UV) and optical light from *Galaxy Evolution Explorer* (*GALEX*), suggests that the error is closer to 0.2 dex for star-forming galaxies (Bundy, private communication).

'Quenched' or 'quiescent' galaxies are those with SFR below $\log {\rm SFR} = 0.74 \log M_* - 8.22$. This division, which was determined by eye, is shown in Fig. 1.

2.4 The group catalogue and halo masses

Yang et al. (2012) constructed a group catalogue and estimated group halo masses for the SDSS DR7 sample based on the

analysis of Yang et al. (2007), and we use this catalogue with a slight modification for self-consistency. We briefly describe their group finder and halo mass estimation below.

The group finder consists of an iterative procedure that estimates the number density contrast of dark matter particles based on the centres, sizes and velocity dispersion of group members, assuming a spherical NFW profile (Navarro, Frenk & White 1997). When they ran their group finder on an SDSS mock catalogue, they successfully selected more than 90 per cent of true haloes more massive than $10^{12}\,\mathrm{M}_{\odot}$.

With their constructed group catalogue, Yang et al. (2007) estimated halo masses by rank-ordering the groups by group stellar mass. They assigned halo masses to the groups by rank, assuming a Λ cold dark matter (ΛCDM) mass function within the observed volume. Running their group-finding and halo abundance matching algorithm on the mock catalogue, they found an rms scatter between real and assigned halo masses of about 0.3 dex.

The stellar masses used by Yang et al. (2007, 2012) are computed using the relations given by Bell et al. (2003), which can underestimate M_* for dusty, star-forming galaxies (for a typical dust model with attenuation of 1.6 and 1.3 in the g and r bands, M_* will be underestimated by 0.2 dex; see Bell et al. 2003). Underestimating M_* for star-forming galaxies but not for quiescent galaxies has the effect of exaggerating quenching trends with M_* at fixed $M_{\rm h}$. Therefore, using the group catalogue of Yang et al. (2012), we recompute group masses using the stellar masses described in Section 2.2, which are estimated via SED fitting that incorporates dust. Note that this calculation does not modify the original group catalogue, i.e. it does not recompute group members based on the new estimates of $M_{\rm h}$ and $R_{\rm vir}$ as done in Yang et al. (2007). In addition to removing biases for specific classes of galaxies, this approach puts the stellar masses for the group galaxies on the same basis as used for the general stellar mass catalogue, thus eliminating systematic errors between them that could eventually percolate into the halo masses.

To account for missing members, we applied the same correction as in Yang et al. (2007), i.e. their $g(L_{19.5}, L_{\rm lim})$ factor, and use the same technique for determining the sample groups that are complete to certain redshifts (refer to their paper for details). Then we computed the Tinker et al. (2008) mass function using the Eisenstein & Hu (1998) transfer function to assign halo masses to the rank-ordered group masses. Our estimates for halo mass are consistent with their estimates above $M_{\rm h} = 10^{12.6}\,\mathrm{M}_{\odot}$. In the range $12.2 < \log M_{\rm h}/\mathrm{M}_{\odot} < 12.6$, our estimates are on average 0.03–0.05 dex higher than theirs, which is expected given that dusty star formers are found in this range.

This catalogue from Yang et al. (2012) contains 633 310 galaxies, of which 176 588 make the redshift, mass and SFFLAG cuts described above. 136 825 reside in haloes with $M_{\rm h} > 10^{11.8}\,\mathrm{M}_{\odot}$. In our analysis we will focus our discussion on those with $M_{\rm h} > 10^{12}\,\mathrm{M}_{\odot}$ since the comparison with the mock catalogue produced acceptable scatter above this limit. Below this, $\log M_{\rm h}$ corresponds more or less one-to-one with the stellar mass of each galaxy since the vast majority of these groups contain one member.

Above $M_{\rm h} < 10^{11.8}\,\mathrm{M}_{\odot}$, 85 749 galaxies are the most massive member of their group (including groups of only one member). Of these, 83 391 are also the nearest galaxy to their mass-weighted centre. We define these galaxies to be 'central' galaxies. The other most massive galaxies are excluded to avoid potentially unrelaxed groups (refer to Carollo et al. 2013; Cibinel et al. 2013).

This leaves 50 963 that are not the most massive member. Of these, a full 29 157 reside in groups in which the most massive member is not the nearest to its group's mass-weighted centre, i.e. in potentially unrelaxed groups. Examining the spatial distribution of a small sample of these groups, we have found that sometimes a small satellite is the nearest to the mass-weighted centre due to projection. Since excluding all galaxies in potentially unrelaxed groups would drastically cut the satellite sample (and unnecessarily for some groups), we decided to define satellites as those that are (1) in 'relaxed' groups (those in which there is a central as defined above) and are not the centrals themselves, or (2) ranked third massive in the group or lower if they are in potentially unrelaxed groups. These criteria yield a sample of 48 598 satellites. The idea behind the second criterion is that the group halo is most likely associated with the two most massive members. However, if we restricted our sample only to the first criterion, our results, though much noisier (after applying the compactness cuts below), would remain qualitatively unchanged.

We define the relative groupcentric distance of satellites as the ratio of the projected distance $d_{\rm proj}$ of each satellite to the mass-weighted group centre and the virial radius $R_{\rm vir} = 120(M_{\rm h}/10^{11}\,\mathrm{M}_{\odot})^{1/3}$ kpc (e.g.Dekel & Birnboim 2006).

2.5 Galaxy compactness

In order to probe quenching mechanisms which result in centrally concentrated galaxies, we compute the surface density within the inner kiloparsec $\Sigma_{1\,\rm kpc}$ in the following way. We retrieved surface brightness profiles in the *ugriz* bandpasses from the SDSS DR7 Catalog Archive Server and corrected them for galactic extinction using the extinction tags in the SpecPhoto table. Then we used the flux within each radial bin and in each band as input into the *K*-correction utilities of Blanton & Roweis (2007), v4_2, to compute the stellar mass profile. We then summed the bins to compute the cumulative stellar mass profile and interpolated between the radial bins to estimate the total mass within 1 kpc and compute the density in this radius.

Out of 897 582 galaxies with profiles retrieved from CasJobs with $z < 0.3$, 133 192 make the cuts described above: 81 063 centrals and 47 524 satellites. None of these had their largest radial bin smaller than 1 kpc, or their smallest radial bin larger than 1 kpc.

This estimate of compactness does not account for contamination from near neighbours. This contamination will be strongest for satellites of large and dense clusters. We checked the importance of this effect on the $\Sigma_{1\,\rm kpc}$–sSFR relation (using an analysis similar to Section 3.1). We find no noticeable difference in the mean trends between galaxies whose nearest photometric neighbour is less than 10 arcsec and those more isolated. Therefore, we do not attempt to correct for this effect.

This estimate also does not correct for inclination, but we have confirmed that applying a selection on inclination ($b/a > 0.5$) does not change our results.

Of potential greater importance is that this computation does not correct for atmospheric seeing. An estimate of the point spread function (PSF) for each galaxy is the effective width of the best-fitting double-Gaussian PSF model in the centre of each SDSS frame (the PSFWIDTH tag in the FIELD table; Fan et al. 2001; Stoughton et al. 2002). Of the 81 063 centrals in our sample, only 7572 are on frames with PSF width less than 1 kpc. These are almost all below $z \sim 0.04$ and include too few high-mass haloes to observe quenching trends with $M_{\rm h}$. Therefore, for the central population, we have selected those galaxies whose PSF widths are less than 2 kpc (57 113 centrals). We discuss the effects of the PSF on our results in Section 3.1 and attempt to correct for it.

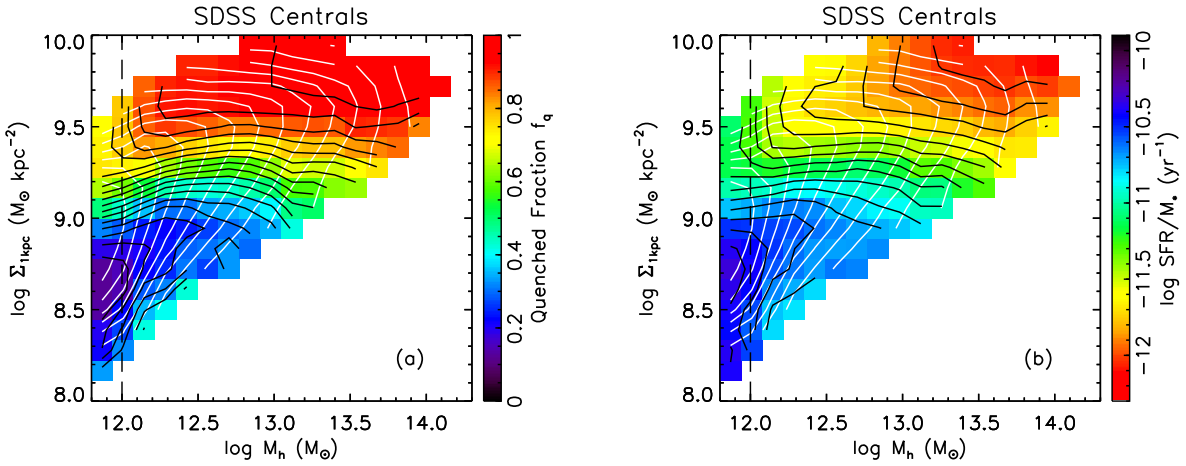

Figure 2. The quenched fraction (a) and the mean log SFR/M_* (b) in the $\Sigma_{1\,\mathrm{kpc}}$–M_h plane for central galaxies after $\Sigma_{1\,\mathrm{kpc}}$ has been corrected for PSF effects as described in Section 3.1. The white contours represent the number density of galaxies per pixel with a maximum of 0.001 Mpc^{-3} and a separation of 0.25 dex. The black contours follow the colour scale and are separated by 0.05 for f_q and 0.12 dex in yr^{-1} for sSFR. The vertical dashed line marks $M_\mathrm{h} = 10^{12}\,\mathrm{M}_\odot$ below which the errors in the M_h estimates increase dramatically, and it also refers to the M_crit near which halo quenching is predicted to become important. The quenched fraction and sSFR for centrals strongly depend on $\Sigma_{1\,\mathrm{kpc}}$ at fixed M_h for mid-range values of $\Sigma_{1\,\mathrm{kpc}}$ ($\sim 10^{9\text{–}9.4}\,\mathrm{M}_\odot\,\mathrm{kpc}^{-2}$). For higher and lower values of $\Sigma_{1\,\mathrm{kpc}}$, there is a gradual decrease in sSFR (and increase in f_q) up to $M_\mathrm{h} \sim 13$. (The same plots without the PSF correction are very similar.)

On the other hand, the satellite population, if limited to those whose PSF widths are less than 1 kpc (8826), will contain objects in massive haloes in sufficient numbers. Thus our analysis of satellites will only include these objects so that our $\Sigma_{1\,\mathrm{kpc}}$ values for these satellites will not be significantly affected by seeing.

Therefore our final sample consists of 57 113 centrals and 8826 satellites.

3 CENTRALS

Here we compare the strength of the quenching correlation with galaxy compactness to the strength of the quenching correlation with halo mass for central galaxies. Fig. 2(a) shows the quenched fraction (represented by the colour scale) a function of the $\Sigma_{1\,\mathrm{kpc}}$–M_h plane for central galaxies. ($\Sigma_{1\,\mathrm{kpc}}$ is corrected for atmospheric seeing according to Section 3.1, but the uncorrected plots are almost indistinguishable.) The white contours show the number density of galaxies per pixel and are separated by 0.25 dex in Mpc^{-3}. The black contours follow the colour scale and are separated by 0.05. The vertical dashed line marks $M_\mathrm{h} = 10^{12}\,\mathrm{M}_\odot$ below which the errors in the M_h estimates increase dramatically (this also happens to be $\sim M_\mathrm{crit}$). Fig. 2(b) is the same as panel (a) except the colour scale represents the mean sSFR, and the black contours are separated by 0.12 dex in sSFR.

This figure shows that for central galaxies with $\Sigma_{1\,\mathrm{kpc}} \sim 10^{9\text{–}9.4}\,\mathrm{M}_\odot\,\mathrm{kpc}^{-2}$, f_q and sSFR are strongly correlated with $\Sigma_{1\,\mathrm{kpc}}$ with only weak M_h dependence. In particular, the range $\Sigma_{1\,\mathrm{kpc}} \sim 10^{9\text{–}9.4}\,\mathrm{M}_\odot\,\mathrm{kpc}^{-2}$ seems to divide the galaxies into those with high sSFR below this range and low sSFR above this range. However, at higher and lower ranges of $\Sigma_{1\,\mathrm{kpc}}$, sSFR and f_q (the latter especially around M_crit) are strong functions of M_h, and mostly independent of $\Sigma_{1\,\mathrm{kpc}}$. These roughly vertical and horizontal contours of quenching in this plane seem to be evidence for two modes of quenching for centrals, one related to the halo and one related to galaxy compactness.

When considering Fig. 2, keep in mind that sSFR is a bimodal quantity and the panels are measuring different aspects of this bimodality. Thus we complement these figures with the entire distribution of sSFR in Figs 3 and 4. In Fig. 3, we show the sSFR distribution for different bins of $\Sigma_{1\,\mathrm{kpc}}$, represented by the different coloured/hashed histograms, in three panels of fixed M_h, which are three vertical slices of Fig. 2(b). This figure shows that varying $\Sigma_{1\,\mathrm{kpc}}$ changes the shape of the sSFR bimodality strongly in that higher $\Sigma_{1\,\mathrm{kpc}}$ results in more galaxies in the quenched peak. This is seen in Fig. 2(a) as a strong increase in f_q. This also explains the strong decrease in mean sSFR with $\Sigma_{1\,\mathrm{kpc}}$ for mid-range values of $\Sigma_{1\,\mathrm{kpc}}$, i.e. the green shaded region in Fig. 2(b). This region does not represent a peak of galaxies in the 'green valley' of the sSFR bimodality, but rather a region where there are comparable numbers of galaxies on either side of the bimodality.

In Fig. 4 we show the sSFR distribution for different bins of M_h, represented by different coloured/hashed histograms, in three panels of fixed $\Sigma_{1\,\mathrm{kpc}}$, which are three horizontal slices of Fig. 2(b). In contrast to $\Sigma_{1\,\mathrm{kpc}}$, this plot shows that varying M_h does not strongly change the shape of the bimodality, but rather shifts the whole distribution of sSFR downward with increasing M_h (at fixed $\Sigma_{1\,\mathrm{kpc}}$). This is seen in Fig. 2(b) as the decrease in sSFR for low and high $\Sigma_{1\,\mathrm{kpc}}$. In fact, the highest bin of M_h for the low-$\Sigma_{1\,\mathrm{kpc}}$ galaxies (the red histogram in Fig. 4a) is not bimodal in sSFR, but rather straddles the 'green valley'. In other words, when quenching by $\Sigma_{1\,\mathrm{kpc}}$ is not present, nor is the bimodality. Halo-related quenching, in the absence of $\Sigma_{1\,\mathrm{kpc}}$ quenching, reduces sSFR more continuously (rather than abruptly shifting the galaxy from star forming to quenched).

It may be noted that the low-sSFR peak in the sSFR bimodality represents more of an upper limit instead of actual measurements of sSFR. The real sSFR values may in fact decrease with increasing $\Sigma_{1\,\mathrm{kpc}}$ even though we do not see this in Fig. 3. However, these upper limits *are* seen to decrease with increasing M_h, showing that M_h more strongly predicts sSFR than $\Sigma_{1\,\mathrm{kpc}}$ for quenched galaxies. At the very least, one can conclude from Figs 3 and 4 (and Fig. 2) that $\Sigma_{1\,\mathrm{kpc}}$ predicts the shape of the distribution of sSFR (i.e. the number of galaxies on either side of the bimodality) whereas M_h predicts the position in sSFR of the entire distribution.

It may also be noted that the different bins of M_h in Fig. 4 also represent different bins of M_* since for central galaxies, these are

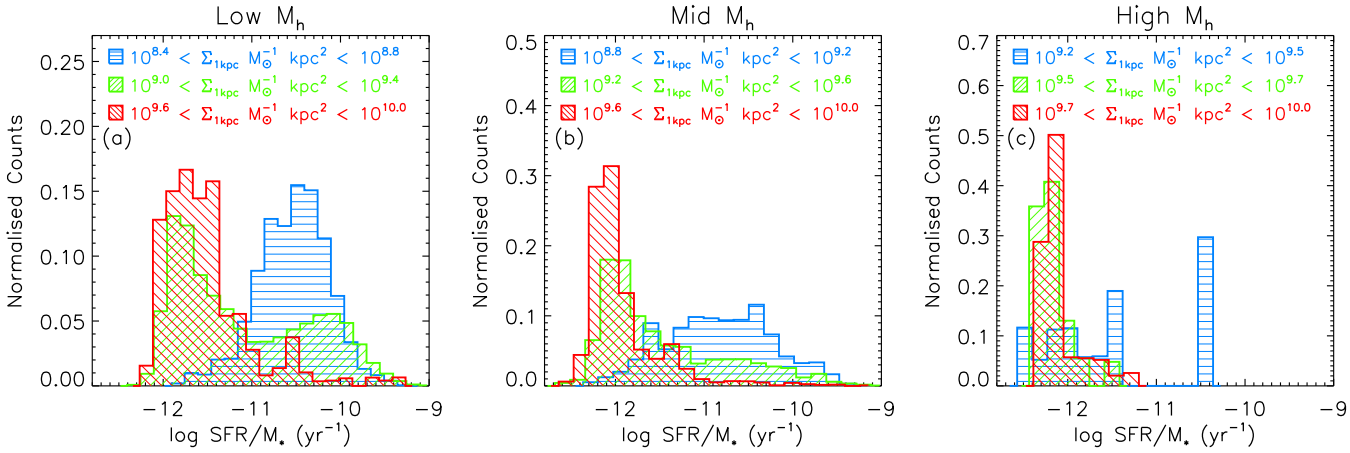

Figure 3. Distribution of sSFR for central galaxies in different bins of $\Sigma_{1\,\mathrm{kpc}}$ (represented by different coloured/hashed histograms) for low (panel a: $12.0 < \log M_\mathrm{h}/\mathrm{M}_\odot < 12.3$), mid-range (panel b: $12.7 < \log M_\mathrm{h}/\mathrm{M}_\odot < 13$) and high (panel c: $13.7 < \log M_\mathrm{h}/\mathrm{M}_\odot < 14$) values of M_h. Varying $\Sigma_{1\,\mathrm{kpc}}$ at fixed M_h changes the relative frequencies of galaxies with high and low sSFR.

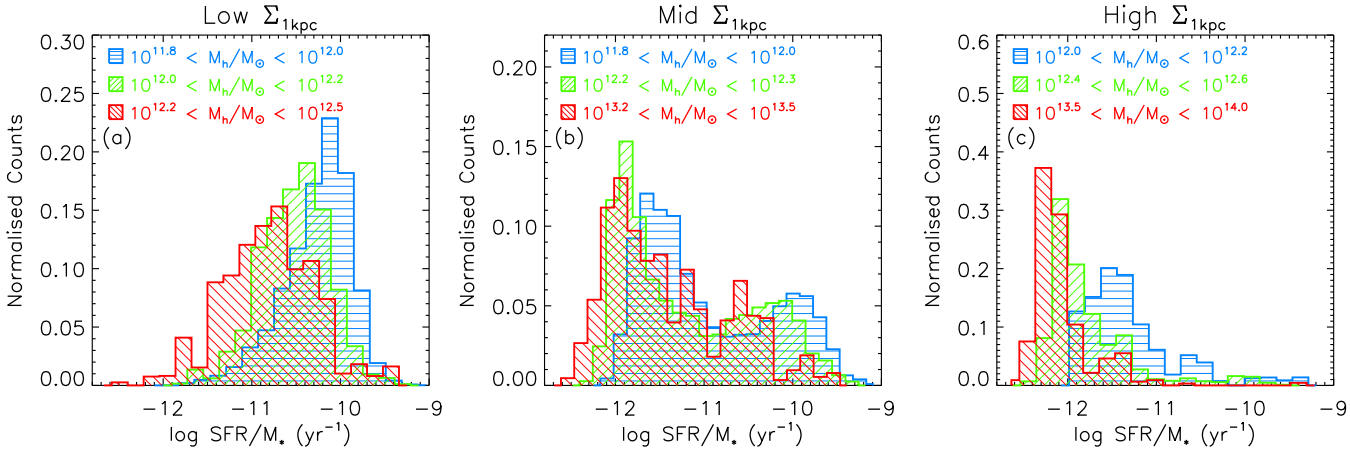

Figure 4. Distribution of sSFR for central galaxies in different bins of M_h (represented by different coloured/hashed histograms) for low (panel a: $8.3 < \log \Sigma_{1\,\mathrm{kpc}}/\mathrm{M}_\odot\,\mathrm{kpc}^{-2} < 8.8$), mid-range (panel b: $9.0 < \log \Sigma_{1\,\mathrm{kpc}}/\mathrm{M}_\odot\,\mathrm{kpc}^{-2} < 9.5$) and high (panel c: $9.6 < \log \Sigma_{1\,\mathrm{kpc}}/\mathrm{M}_\odot\,\mathrm{kpc}^{-2} < 10$) values of $\Sigma_{1\,\mathrm{kpc}}$. Varying M_h at fixed $\Sigma_{1\,\mathrm{kpc}}$ shifts the whole distribution of sSFR to lower values without a significant change in its shape.

closely correlated. (The fixed bins of M_h in each panel of Fig. 3 do represent roughly fixed bins of M_*.) Thus a shift of the sSFR distribution shows that the downward slope of the sSFR–M_* relation is still negative after selecting galaxies with a fixed $\Sigma_{1\,\mathrm{kpc}}$. However, we show in Fig. 5 that M_h also reduces sSFR independently of M_*. Panel (a) shows the distribution of sSFR for the same range of $\Sigma_{1\,\mathrm{kpc}}$ as in Fig. 4(b), but also for fixed M_* ($10^{10.3\text{–}10.6}\,\mathrm{M}_\odot$). Since we have greatly reduced the sample, the distributions are rather noisy, so we also show the cumulative distribution of sSFR in Fig. 5(b). These panels show that even at fixed M_* and fixed $\Sigma_{1\,\mathrm{kpc}}$, increasing halo mass seems to shift the sSFR distribution to lower values. The same shift is seen when restricting the M_* ranges of Figs 4(a) and (c). A two-sided Kolmogorov–Smirnov test shows that the probability that the red and blue histograms in Fig. 5 are drawn from the same distribution is less than 10^{-5}. We also performed the same analysis on the distribution of ΔsSFR, i.e. the distance of the sSFR from the dividing line in Fig. 1 and find the similar results.

To further explore the role of M_* in determining sSFR, we show in Fig. 6 the cumulative distribution in three bins of M_* in a slice of both $\Sigma_{1\,\mathrm{kpc}}$ ($10^{9\text{–}9.5}\,\mathrm{M}_\odot\,\mathrm{kpc}^{-2}$) and M_h ($10^{12.0\text{–}12.3}\,\mathrm{M}_\odot$). The three distributions lie on top of each other. A two-sided Kolmogorov–Smirnov test shows that the probability that the red and blue histograms are drawn from the same distribution is as high as 0.13. However, note that fixing the range of M_h leaves only a small range of M_* in contrast to the other way around (Fig. 5) due to the shape of the M_*–M_h relation (Yang et al. 2007; Moster et al. 2010; Woo et al. 2013). Thus M_* seems to provide no additional information for quenching to the combination of $\Sigma_{1\,\mathrm{kpc}}$ and M_h, whereas M_h does add information over M_* (Fig. 5), in agreement with Woo et al. (2013).

How important is halo quenching? About 36 per cent of diffuse galaxies with $12.2 < \log M_\mathrm{h}/\mathrm{M}_\odot < 12.5$ are quenched (red histogram of Fig. 4 a). Assuming that $\Sigma_{1\,\mathrm{kpc}}$-related quenching and halo quenching are the only quenching mechanisms, these are quenched by the halo alone. Furthermore, of all the quenched galaxies in Fig. 2 (namely $M_\mathrm{h} > 10^{11.8}\,\mathrm{M}_\odot$), 21 per cent lie below $\Sigma_{1\,\mathrm{kpc}} = 10^9\,\mathrm{M}_\odot\,\mathrm{kpc}^{-2}$ and these must be quenched by the halo alone. (Since the threshold mass for halo quenching can vary over a wide range around $10^{12}\,\mathrm{M}_\odot$, some of the haloes of $\sim 10^{11.8}\,\mathrm{M}_\odot$ can easily be quenching via the halo.)

Similarly, those that are quenched by $\Sigma_{1\,\mathrm{kpc}}$-related processes alone would be those with mid-to-high $\Sigma_{1\,\mathrm{kpc}}$ and low M_h, such as the left-hand peak of the blue histograms in Figs 4(b) and (c). Of all quenched galaxies in Fig. 2, 35 per cent are above

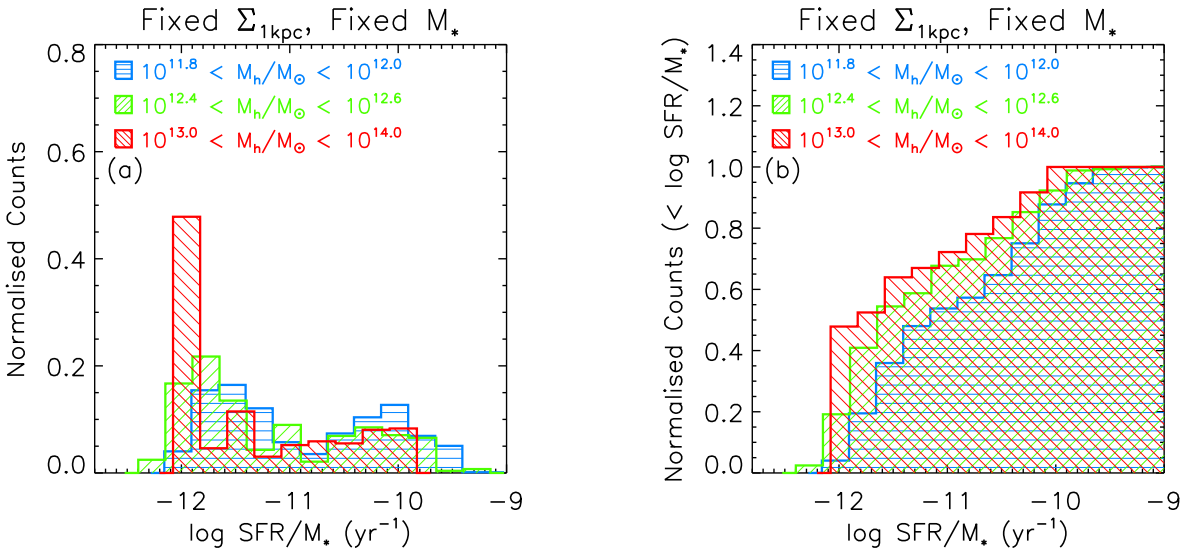

Figure 5. The distribution of sSFR (a) and the cumulative distribution of sSFR (b) for central galaxies at fixed $\Sigma_{1\,\mathrm{kpc}}$ ($9 < \log \Sigma_{1\,\mathrm{kpc}}/\,\mathrm{M}_\odot\,\mathrm{kpc}^{-2}$) and fixed M_* ($10.3 < \log M_*/\,\mathrm{M}_\odot < 10.6$) for different bins of M_h, represented by the different coloured/hashed histograms. Increasing M_h seems to shift the sSFR distribution to lower values.

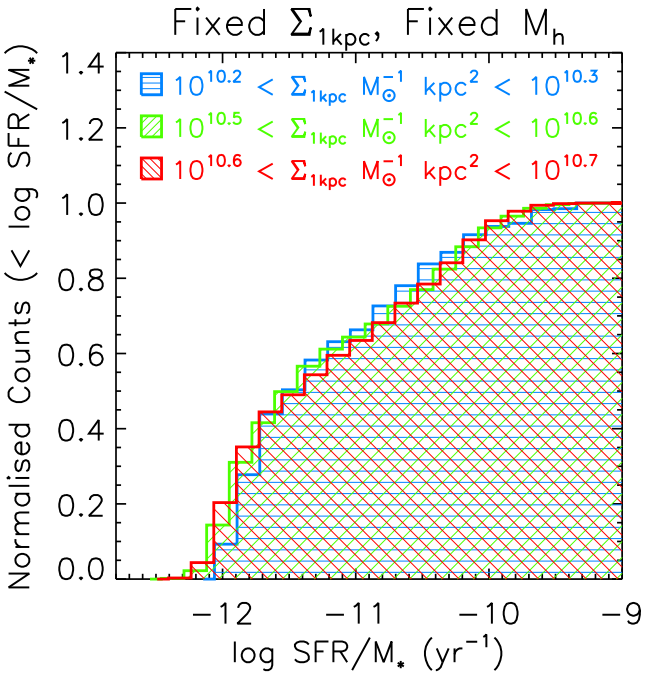

Figure 6. The cumulative sSFR distribution in three bins of M_* after fixing $\Sigma_{1\,\mathrm{kpc}}$ ($10^{9\text{–}9.5}\,\mathrm{M}_\odot\,\mathrm{kpc}^{-2}$) and fixing M_h ($10^{12.0\text{–}12.3}\,\mathrm{M}_\odot$). M_* does not significantly alter the sSFR distribution.

$\Sigma_{1\,\mathrm{kpc}} = 10^9\,\mathrm{M}_\odot\,\mathrm{kpc}^{-2}$ and below $M_\mathrm{h} = 10^{12}\,\mathrm{M}_\odot$. These can be suspected of being quenched by $\Sigma_{1\,\mathrm{kpc}}$-related quenching only, not yet being in massive enough haloes for maintaining halo quenching. However, M_h for these galaxies is high enough for the halo to possibly also play a role in their quenching.

Most of the quenched centrals have both high $\Sigma_{1\,\mathrm{kpc}}$ and high M_h (79 per cent with $\Sigma_{1\,\mathrm{kpc}} > 10^9\,\mathrm{M}_\odot\,\mathrm{kpc}^{-2}$ and $M_\mathrm{h} > 10^{11.8}\,\mathrm{M}_\odot$). These seem to have experienced both quenching mechanisms, though one may have occurred before the other.

These results taken together point to the presence of both compactness-related quenching and halo quenching, and to the nature of their quenching roles. If the increase of f_q measures the transfer of galaxies from one side of the galaxy bimodality to the other, while the decrease of sSFR relates to the fading of star formation, then for central galaxies, the process related to compactness plays the transferring role, while the halo plays the fading role. This will be discussed further in Section 5.

3.1 The effect of atmospheric seeing

Since we have not limited the sample of centrals to those where the PSF width is less than 1 kpc (but rather to those for which the PSF width is less than 2 kpc), it is important to discuss potential effects that atmospheric seeing may have on our results. Since the PSF tends to move light outward in monotonically decreasing surface brightness profiles, uncorrected profiles will underestimate $\Sigma_{1\,\mathrm{kpc}}$. Furthermore, since the PSF width is smaller in red bandpasses than in blue bandpasses, this could potentially have one or both of two opposite consequences. First, the uncorrected $\Sigma_{1\,\mathrm{kpc}}$ for blue galaxies will be underestimated to a greater degree than for red galaxies. In other words, if colour roughly translates to sSFR, the effect of seeing is to artificially raise the mean sSFR in low bins of $\Sigma_{1\,\mathrm{kpc}}$. Similarly, if colour roughly translates to the quenched fraction, the effect of seeing is to artificially steepen the gradient of f_q with $\Sigma_{1\,\mathrm{kpc}}$. Second, in a given galaxy, bluer light moves outward more than red light, leaving its centre appearing redder, and thus appearing to have higher mass-to-light ratio. Thus, the PSF can artificially raise $\Sigma_{1\,\mathrm{kpc}}$.

How important are these effects? One way to measure this is to look at the mean $\Sigma_{1\,\mathrm{kpc}}$ as a function of sSFR, comparing galaxies with good PSF widths (<1 kpc) to galaxies with large PSF widths (>1 kpc). We show this comparison in Fig. 7 in several bins of M_*. The red triangles are those with good PSF widths, and the black squares are those with large PSF widths. This figure shows that galaxies with high sSFR (i.e. those that are bluer) have higher measured $\Sigma_{1\,\mathrm{kpc}}$ when the PSF widths are small compared to those whose PSF widths are large. In other words, the PSF causes an underestimate of $\Sigma_{1\,\mathrm{kpc}}$ for bluer galaxies as expected. The difference between the mean $\Sigma_{1\,\mathrm{kpc}}$ is at the most about 0.1 dex and is larger

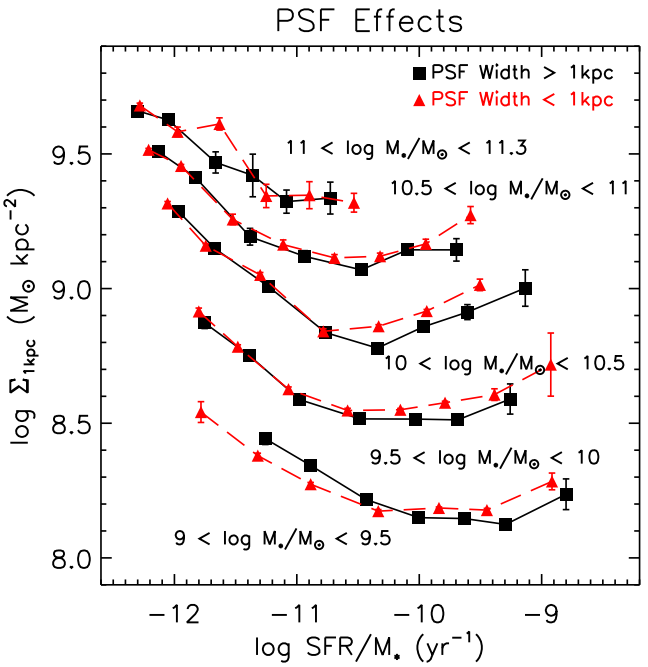

Figure 7. Measured values of the mean $\Sigma_{1\,\mathrm{kpc}}$ as a function of sSFR and M_* comparing those galaxies whose PSF widths are larger than 1 kpc (black squares) to those galaxies whose PSF widths are smaller than 1 kpc (red triangles). The error bars are errors on the mean. The effect of seeing is to underestimate the measured $\Sigma_{1\,\mathrm{kpc}}$, especially for low-mass star-forming (blue) galaxies. The large PSF group of low-mass passive galaxies has higher $\Sigma_{1\,\mathrm{kpc}}$ than the small PSF group, likely because the former includes galaxies at higher z where low surface brightness galaxies drop from the sample.

for less massive galaxies. For the lowest mass bin, Fig. 7 also shows that galaxies with low sSFR have higher measured $\Sigma_{1\,\mathrm{kpc}}$ when the PSF is large compared to those whose PSF is small (i.e. the black line is higher than the red line). These may either be because of the second effect of the PSF described above, or because the large PSF group on average higher z (within the same z bin) where low surface brightness galaxies drop from the sample.

Thus, to create Fig. 2, we estimated a correction to $\Sigma_{1\,\mathrm{kpc}}$ based on Fig. 7. For each bin of log M_*, we calculated the difference between the red and black lines in Fig. 7. This difference is an increasing function of log sSFR which is roughly linear. A linear least-squares fit to the differences resulted in an approximate upward correction to $\Sigma_{1\,\mathrm{kpc}}$ as a function of sSFR in bins of M_*. We applied this correction to those galaxies whose PSF widths are larger than 1 kpc.

After applying these rough corrections, we compared Fig. 2 to the same plot without corrections (not shown here) and find that the differences are almost imperceptible. Thus the PSF seems to have a small effect on the broad trends of f_q and sSFR for most of the $\Sigma_{1\,\mathrm{kpc}}$–M_h plane if we select PSF widths <2 kpc (which is our sample of centrals). The most significant change is that the mean f_q is slightly lowered (by less than 0.05) at high $\Sigma_{1\,\mathrm{kpc}}$ below $M_\mathrm{h} \sim 10^{12}\,\mathrm{M}_\odot$. We expect the PSF effects to become more significant for selections that include larger PSF widths and higher z.

4 SATELLITES

Woo et al. (2013) showed that the quenched fraction for satellites depend strongly on groupcentric distance $d_\mathrm{proj}/R_\mathrm{vir}$ and M_h. These authors showed that f_q also depends on M_*, but only in the outer regions of groups. Position in the host halo correlates with time after infall so this result suggests that satellites behave as centrals (ignoring the host halo) for some time after they fall in (Wetzel, Tinker & Conroy 2012).

62 per cent of satellites reside in the outer regions ($\log(d_\mathrm{proj}/R_\mathrm{vir}) > -0.5$) while only 8 per cent of them live in the inner regions ($\log(d_\mathrm{proj}/R_\mathrm{vir}) < -1$). Therefore quenching studies which do not separate satellites into regional bins (or even worse, combine all centrals and satellites) will miss the strong M_h signal seen in Woo et al. (2013). Therefore, when comparing the effects of the halo and galaxy compactness on quenching, we must keep these regional differences in mind.

Fig. 8 (top) shows the quenched fraction of satellites as a function of the $\Sigma_{1\,\mathrm{kpc}}$–M_h plane in three bins of $d_\mathrm{proj}/R_\mathrm{vir}$. This figure shows that f_q strongly depends on $\Sigma_{1\,\mathrm{kpc}}$ for satellites in the outer regions of groups, just as it does for centrals. However even here in the outer halo, the influence of the host halo is non-negligible since f_q increases slightly with M_h at fixed $\Sigma_{1\,\mathrm{kpc}}$. The M_h dependence of the quenched fraction becomes much more dominant in the inner regions of haloes where the $\Sigma_{1\,\mathrm{kpc}}$ dependence of f_q almost disappears.

Note also that the quenched fraction reaches ∼50 per cent at $\sim 3 \times 10^{12}\,\mathrm{M}_\odot$, while nearly all satellites in the inner halo are quenched above $M_\mathrm{h} \sim 10^{13}\,\mathrm{M}_\odot$. The difference may reflect the long duration of halo quenching (more on this in Section 5).

Just as for the centrals, these results are evidence for two modes of quenching, one related to $\Sigma_{1\,\mathrm{kpc}}$ and one related to the halo, which influences satellites differently in different regions of the halo. To further understand what roles the halo and galaxy structure play in quenching, we show the mean sSFR for satellites in Fig. 8 (bottom) as a function of $\Sigma_{1\,\mathrm{kpc}}$ and M_h, divided in the same bins of groupcentric distance.

Fig. 8 (bottom) shows that while the behaviour of sSFR is similar to f_q in the outer and intermediate halo, the decrease of sSFR with $\Sigma_{1\,\mathrm{kpc}}$ is enhanced for satellites in the inner regions of $\gtrsim 10^{13}\,\mathrm{M}_\odot$ haloes. Although all these satellites are formally quenched (top panel), many appear to be near the borderline. For those, $\Sigma_{1\,\mathrm{kpc}}$ is still able to modulate sSFR, as shown in the bottom panel.

The environmental trends in Fig. 8 are independent of any relation between $\Sigma_{1\,\mathrm{kpc}}$ and $d_\mathrm{proj}/R_\mathrm{vir}$ because a horizontal strip in this figure is a strip of constant $\Sigma_{1\,\mathrm{kpc}}$. In one such strip, say $\log \Sigma_{1\,\mathrm{kpc}} = 9$, f_q (and sSFR) above $M_\mathrm{h} = 10^{13}\,\mathrm{M}_\odot$ increases (decreases) towards the inner halo. However, we show explicitly in Fig. 9 that $\Sigma_{1\,\mathrm{kpc}}$ varies only weakly with distance. This plot shows $\Sigma_{1\,\mathrm{kpc}}$ as a function of $d_\mathrm{proj}/R_\mathrm{vir}$ in bins of M_*. Clearly, $\Sigma_{1\,\mathrm{kpc}}$ varies only weakly with $d_\mathrm{proj}/R_\mathrm{vir}$ for all masses. At the most, $\Sigma_{1\,\mathrm{kpc}}$ increases by about 0.1 dex between R_vir and $0.1R_\mathrm{vir}$ which is smaller than the size of one of the pixels in Fig. 8.

Fig. 8 includes satellites of all masses. We investigate quenching in the $\Sigma_{1\,\mathrm{kpc}}$–M_h plane for satellites in two narrow bins of M_* in Fig. 10. These mass bins turn out to be two horizontal slices of Fig. 8 since $\Sigma_{1\,\mathrm{kpc}}$ and M_* are strongly correlated. The coloured shading shows f_q, but sSFR is very similar. These narrow slices of M_* contain too few satellites with $\log(d_\mathrm{proj}/R_\mathrm{vir}) < -1.0$ (the inner halo) to make any meaningful conclusions, so we omit this distance bin in Fig. 10. The black contours in both M_* bins are nearly horizontal in the outer halo and steepen in the intermediate halo. The difference in the quenching contours between the different regions of the halo is greater for less massive satellites, but even massive galaxies feel the effects of the halo at intermediate distances.

These results taken together show that halo-related quenching is important in determining f_q for satellites in the inner regions of haloes. Quenching that correlates with galaxy structure, which is

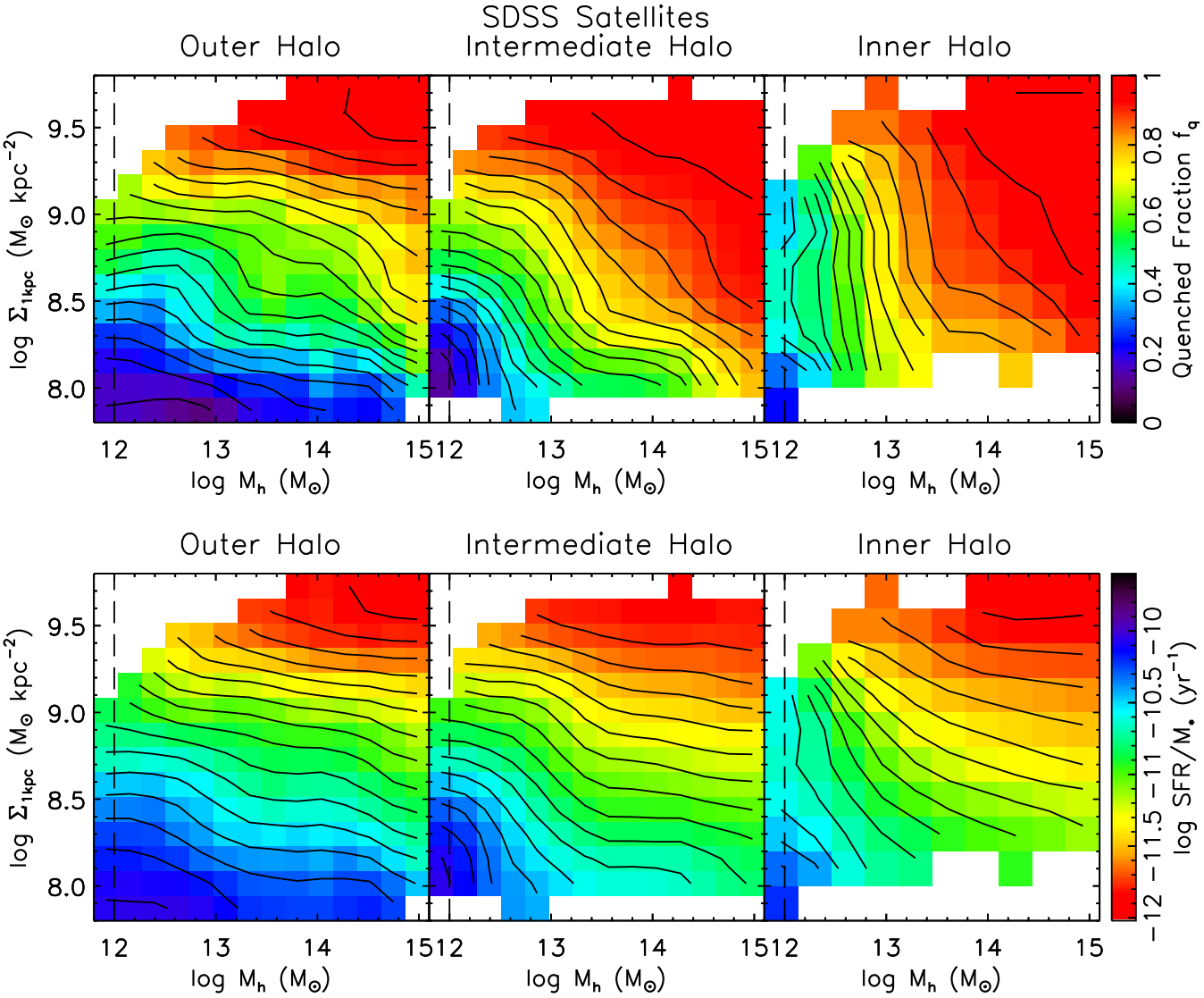

Figure 8. The quenched fraction (top) and sSFR (bottom) of satellites as a function of the $\Sigma_{1\,\mathrm{kpc}}$–M_h plane in three bins of groupcentric distance. The 'outer halo' refers to $\log(d_\mathrm{proj}/R_\mathrm{vir}) > -0.5$, 'intermediate halo' refers to $-1.0 < \log(d_\mathrm{proj}/R_\mathrm{vir}) < -0.5$ and the 'inner halo' refers to $\log(d_\mathrm{proj}/R_\mathrm{vir}) < -1.0$. This sample is limited to only those satellites for which 1 kpc is greater than the PSF width. The white contours represent the number density of galaxies per pixel and are separated by 0.25 dex in Mpc^{-3} with maxima of 8×10^{-4}, 4×10^{-4} and 8×10^{-5} Mpc^{-3} in each panel from left to right. The black contours follow the colour scale and are 0.05 apart for f_q and 0.12 dex in yr^{-1} for sSFR. The vertical dashed line marks $M_\mathrm{h} = 10^{12}\,\mathrm{M}_\odot$ below which the errors in the M_h estimates increase dramatically. f_q depends predominantly on M_h in the inner regions of haloes, while sSFR depends on both M_h and $\Sigma_{1\,\mathrm{kpc}}$ in this region.

most important in the outer halo, also plays a role in the inner halo in determining the satellites' mean sSFR. We discuss a possible interpretation of these results in Section 5.

5 DISCUSSION

5.1 Two types of quenching

Our results suggest that both the halo and inner galaxy compactness play a role in the quenching of central and satellite galaxies. For centrals, f_q increases strongly with $\Sigma_{1\,\mathrm{kpc}}$ while the halo shifts the entire sSFR distribution. Most quenched centrals are both compact and have massive haloes, but one in five quenched centrals above $M_\mathrm{h} = 10^{11.8}\,\mathrm{M}_\odot$ are diffuse ($\Sigma_{1\,\mathrm{kpc}} < 10^9\,\mathrm{M}_\odot\,\mathrm{kpc}^{-2}$), indicating that they were not quenched via $\Sigma_{1\,\mathrm{kpc}}$-related processes. For satellites $\Sigma_{1\,\mathrm{kpc}}$ dominates quenching on the outskirts of haloes while the halo dominates satellite quenching near the halo centre.

These findings are consistent with other observational work confirming the importance of the bulge/central compactness in the quenching of galaxies (Bell 2008; Wuyts et al. 2011; Bell et al. 2012; Cheung et al. 2012; Barro et al. 2013; Omand et al. 2014) and the importance of the halo in quenching (Weinmann et al. 2006; Woo et al. 2013; Tal et al. 2014). Fang et al. (2013) also find that both $\Sigma_{1\,\mathrm{kpc}}$ and stellar mass M_* of central galaxies are important predictors of quenching. Since M_* for centrals is a only crude proxy for the halo mass, we have added to the discussion by examining the role of the halo directly, as well as comparing the quenching roles of mass and compactness for satellites. Our results are also consistent with those of Bluck et al. (2014). They show that f_q increases with bulge mass (which is correlated with $\Sigma_{1\,\mathrm{kpc}}$) at constant M_h (their fig. 11), and with M_h at constant bulge mass (but not with M_* – their

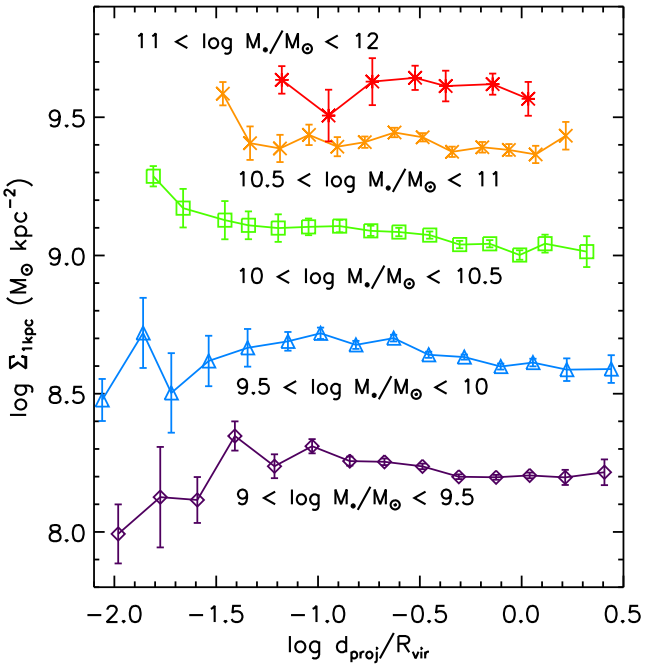

Figure 9. Mean $\Sigma_{1\,\mathrm{kpc}}$ as a function of $d_{\mathrm{proj}}/R_{\mathrm{vir}}$ in bins of M_*. The error bars are errors on the means. $\Sigma_{1\,\mathrm{kpc}}$ varies only weakly with $d_{\mathrm{proj}}/R_{\mathrm{vir}}$ for all masses, increasing at the most by 0.1 dex between R_{vir} and $0.1R_{\mathrm{vir}}$.

fig. 13). Note that they do not point out the latter trend of f_{q} with M_{h} which is clearly visible in their fig. 13, but emphasize that the former trend is strongest.

How shall we interpret these results, and in particular the different behaviours of f_{q} and sSFR? We propose that the increase of f_{q} is related to the transfer of galaxies from one side of the galaxy bimodality to the other since it measures the fraction of galaxies that are on one side. The time-scale for this transfer must be short so as not to fill up the 'green valley' (see Fig. 3). In contrast, the decrease of sSFR refers to a slower fading of star formation. Thus the quenching processes that are related to compactness are quick while the halo process is slow.[2]

Halo quenching is expected to operate in haloes of masses above a threshold mass M_{crit} of order $10^{12}\,\mathrm{M}_{\odot}$, where the cooling time is longer than the relevant dynamical time. This enables a stable shock at the virial radius, behind which the gas heats to the virial temperature, such that gas supply to the central galaxy shuts off (Dekel & Birnboim 2006; Birnboim & Dekel 2003). While the virial shock heating in a given halo could be quick, M_{crit} is expected to vary by an order of magnitude between different haloes because of their different histories. For example, M_{crit} depends on metallicity, which varies from halo to halo (Dekel & Birnboim 2006, fig. 2). Furthermore, once the halo mass is in the vicinity of $\sim M_{\mathrm{crit}}$, our simulations demonstrate that in many cases the development of a virial shock awaits a trigger, e.g. by a minor merger. Indeed, simulations show that the hot gas fraction is increasing very gradually with halo mass, growing from $\ll 1$ to ~ 1 over almost two orders of magnitudes in M_{h} about M_{crit} (Kereš et al. 2005, 2009; Birnboim, Dekel & Neistein 2007; Ocvirk et al. 2008; van de Voort et al. 2011). This predicted behaviour of halo quenching is consistent with the weak dependence of f_{q} and sSFR on M_{h} (at fixed $\Sigma_{1\,\mathrm{kpc}}$) for centrals.

Once all the halo gas is heated, cold gas that is already present within the galaxy[3] is expected to continue forming stars until all the gas is consumed or lost by feedback-driven outflows. The typical gas depletion time for massive galaxies is ∼2–3 Gyr (or longer for early-type Sa discs) in the local universe (Pflamm-Altenburg & Kroupa 2009; Bigiel et al. 2011; Saintonge et al. 2011), and at $z \sim 1$–2 (Saintonge et al. 2011; Dekel & Krumholz 2013; Dekel & Mandelker 2014). Therefore we expect the shutdown of the gas supply to be manifested in a slow fading of star formation, or a decrease in sSFR. This is consistent with the decrease in sSFR with M_{h} for central galaxies. This slower fading produces a continuous, rather than bimodal, distribution of sSFR as seen in the absence of $\Sigma_{1\,\mathrm{kpc}}$-related quenching (red histogram of Fig. 4a).

On the other hand, bulge-building/compacting mechanisms that may result in quenching, such as major mergers and gaseous inflows through disc instability, especially at high-z, are inherently violent. The resulting starbursts lower the gas depletion time-scales in ongoing mergers (and probably also during violent disc instability) by factors of 4 to >10 (Young et al. 1986; Sanders, Scoville & Soifer 1991; Sanders & Mirabel 1996; Gao & Solomon 2004). Powerful outflows due to the stellar winds from these starbursts or from AGN fed by the gaseous inflows may further decrease the depletion time. Thus we expect quenching through these mechanisms to occur quickly compared to halo shock heating. Their quick nature may also imply that most galaxies that quench through these processes quench at high-z (Dekel & Burkert 2014). Indeed, in hydrodynamical zoom-in simulations, Zolotov et al. (2014) find that quenching driven by compaction via instabilities takes less than a 1 Gyr. Quick bulge/compaction-related quenching is consistent with our observation that f_{q} increases primarily with $\Sigma_{1\,\mathrm{kpc}}$ while sSFR for the star-forming and quenched galaxies does not. While such processes seem to be rare at $z = 0$ (Yesuf et al. 2014), many quenched galaxies observed today with high $\Sigma_{1\,\mathrm{kpc}}$ may have quenched at high-z.

However, once gas in consumed in a bulge-building/compacting starburst and associated outflows, there must be a mechanism for preventing new cold gas from accreting on to the galaxy in order to maintain its quenched state. The halo may play this role. Thus the overall 'ripeness' for quenching may be set by the halo while the moment of (quick) transition is triggered by internal, $\Sigma_{1\,\mathrm{kpc}}$-related processes.

Our result that galaxies with high $\Sigma_{1\,\mathrm{kpc}}$ in haloes less massive than $10^{12}\,\mathrm{M}_{\odot}$ have lower f_{q} and higher sSFR than those in more massive haloes (upper left-hand corner of both panels of Fig. 2) may be evidence that $\Sigma_{1\,\mathrm{kpc}}$-related processes are not enough to quench galaxies, and that the halo is needed for quenching maintenance. Indeed, most quenched centrals are both compact and in massive haloes. Our finding that sSFR decreases with M_{h} for high-$\Sigma_{1\,\mathrm{kpc}}$ galaxies may also point to an increased efficiency of 'radio mode' AGN feedback in hotter, more massive haloes (Kormendy & Ho 2013 and references therein). Galaxies with low $\Sigma_{1\,\mathrm{kpc}}$ are not undergoing quick structure-related quenching, and so these galaxies are an opportunity to observe the slower M_{h}-dependent quenching by itself. Indeed for these, we observe that both sSFR and f_{q} correlate with M_{h}. Thus, for those galaxies which experience both quenching mechanisms, the quicker compaction-related processes

[2] Some may consider only the former as 'quenching', and the latter more as star formation regulation. However, since the halo mechanism is thought to shutdown gas accretion which would otherwise continue to feed star formation, we will continue to refer to this also as 'quenching' in this discussion.

[3] Cold streams at $z > 1$–2 may still bring gas into the most massive galaxies even in shock-heated haloes (Dekel et al. 2009).

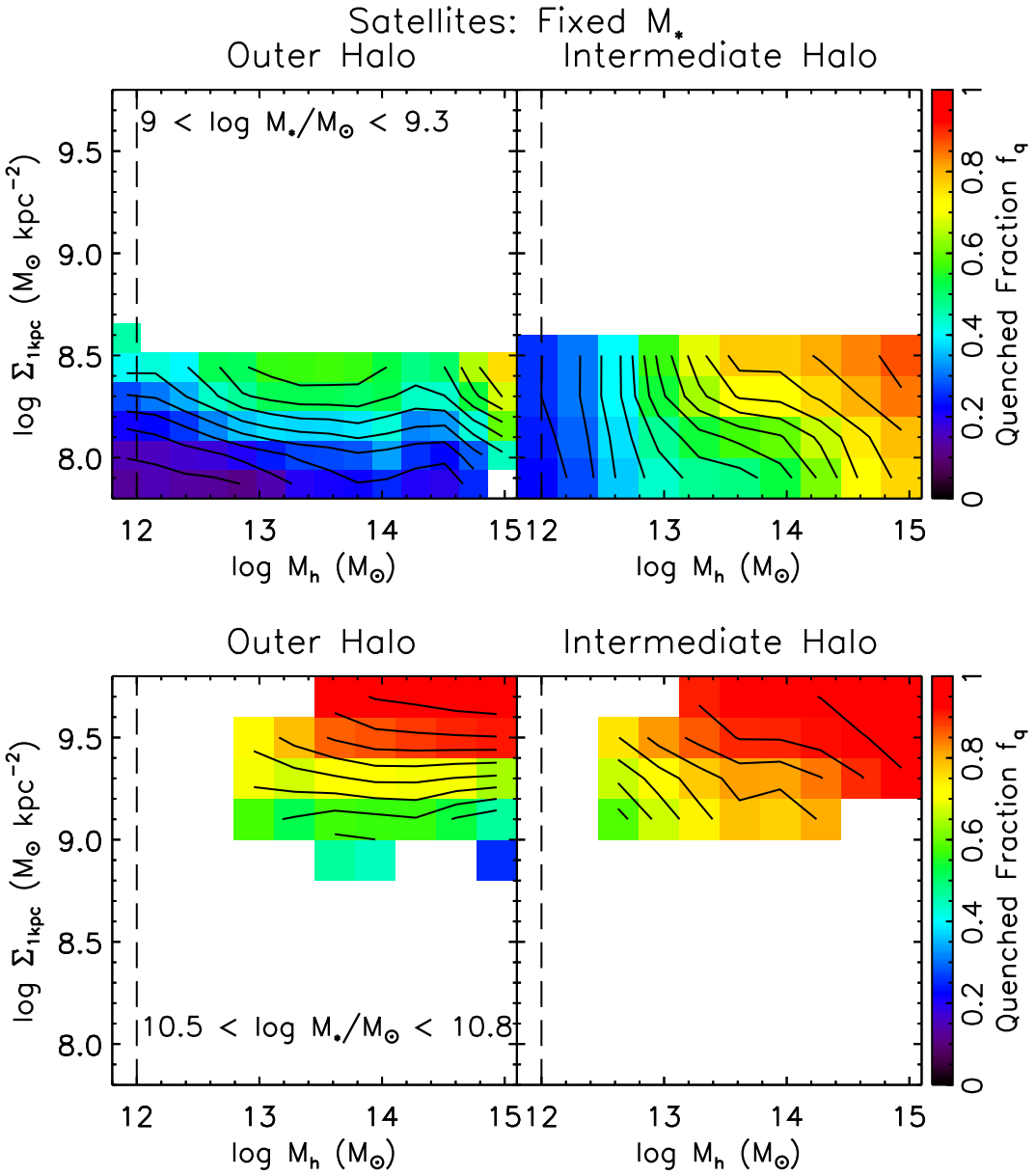

Figure 10. The quenched fraction (top) and sSFR (bottom) of satellites as a function of the $\Sigma_{1\,\mathrm{kpc}}$–M_h plane in two bins of groupcentric distance and two bins of M_*. The 'outer halo' refers to $\log(d_\mathrm{proj}/R_\mathrm{vir}) > -0.5$, and the 'intermediate halo' refers to $-1.0 < \log(d_\mathrm{proj}/R_\mathrm{vir}) < -0.5$. This sample is limited to only those satellites for which 1 kpc is greater than the PSF width. The black contours follow the colour scale and are 0.05 apart for f_q and 0.12 dex in yr^{-1} for sSFR. The vertical dashed line marks $M_\mathrm{h} = 10^{12}\,\mathrm{M}_\odot$ below which the errors in the M_h estimates increase dramatically. The steepening of the f_q–M_h relation in the intermediate halo (relative to the outer halo) is stronger for less massive satellites.

may play the role of triggering quenching while the slower halo process plays the maintenance role.

Since the majority of quenched centrals are both compact and in massive haloes, it may also be possible that the dominant quenching mode is a single process related to both compactness and massive haloes, rather than two independent channels with two different time-scales. After all, the two are strongly correlated. However, this work demonstrates that the halo and compactness work independently. The evidence for their independence is in the observed quenching of centrals in massive haloes that are diffuse, and of compact centrals that are in low-mass haloes. Thus, rather than postulating a third (more dominant) channel where the halo and compactness are linked, we have preferred the simpler scenario that these two independent channels work best together. Distinguishing between these scenarios is beyond the scope of this work.

Not addressed by this analysis are the galaxies that seem to be quenching slowly and also building a dense bulge (slowly e.g. pseudo-bulges). These bulges may only be incidentally growing while their star formation is slowly fading due to the halo. A study of the halo and bulge properties (classical versus pseudo-bulges) of galaxies moving slowly through the green valley is needed to answer this question.

Also important is the fact that a significant area of the $\Sigma_{1\,\mathrm{kpc}}$–M_h plane is strongly bimodal in sSFR. This means that the combination of $\Sigma_{1\,\mathrm{kpc}}$ and M_h does not perfectly predict quenching, and there remains at least one other unknown quantity important for

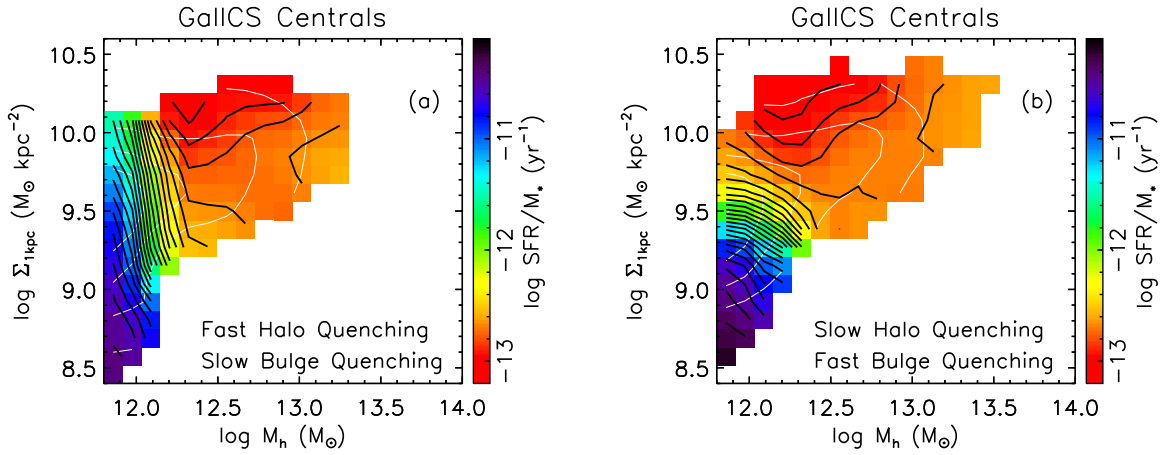

Figure 11. Mean log SFR/M_* as a function of $M_{\rm h}$ and $\Sigma_{1\,{\rm kpc}}$ in the GALICS SAM at $z = 0$. Quenching in panel (a) is implemented such that halo quenching cuts off accretion and removes gas from the central galaxy while bulge quenching only cuts off accretion. In panel (b), quenching is implemented such that halo quenching only cuts off accretion while bulge quenching both cuts off accretion and removes gas from the central galaxy. The white contours represent the number density of galaxies per pixel and are separated by 0.25 dex in Mpc^{-3}. The black contours follow the colour scale and are 0.12 dex apart in yr^{-1}. The contours of sSFR in panel (b) are qualitatively more similar to Fig. 2(b) than panel (a).

quenching. This is related to the phenomenon of 'galactic conformity' (Weinmann et al. 2006; Hartley et al. 2014; Knobel et al. 2014) which states, among other things, that $M_{\rm h}$ does fully describe the quenched state of galaxies in a halo. Quenching is correlated with $\Sigma_{1\,{\rm kpc}}$ and $M_{\rm h}$, but possible time delays in quenching make the physical mechanisms very hard to track.

Despite these uncertainties, however, the picture of quick $\Sigma_{1\,{\rm kpc}}$-related quenching and the halo regulating the slower fading of star formation seems to be a good first-order fit to our observations.

5.2 A SAM test

The interpretation that the different durations of halo-related quenching and compactness/bulge-related quenching mechanisms are responsible for the observed quenching trends for centrals can be tested via semi-analytic modelling. We performed a preliminary analysis of the GALICS semi-analytic model (SAM; Hatton et al. 2003; Cattaneo et al. 2007, 2008, 2013) to test this and the results are encouraging.

The GALICS SAM runs on N-body merger trees of dark matter. The baryonic prescription which populates the haloes with galaxies and evolves them is nearly identical to that of Cattaneo et al. (2013). In brief, gas is cooled on to discs whose sizes are determined by conserving angular momentum. Star formation is activated when the gas surface density reaches the Kennicutt threshold (Kennicutt 1989, 1998). Bulges are grown via mergers and disc instabilities which transfer mass from the disc to the bulge, passing through a starburst phase. The amount of mass transferred is a function of the merger ratio, or the amount that stabilizes the disc in the case of a disc instability. Stellar feedback returns mass and metals to the cold medium. Supernova energy returns cold gas to the hot medium or ejects gas depending on the deepness of the potential well.

GALICS implements both halo-related quenching and bulge-related quenching. Halo-related quenching is implemented by imposing a critical halo mass $M_{\rm crit}$ ($=10^{12}\,{\rm M}_\odot$ and increases with z above $z = 3.2$ according to Dekel & Birnboim 2006), above which accretion is cut off and all gas is removed from the galaxy. That is, halo quenching is implemented to be immediate. In contrast, for galaxies with bulge-to-total mass ratio $B/T > 0.5$, only accretion is halted and remaining gas is allowed to continue forming stars. Thus, GALICS implements both halo- and bulge-related quenching with durations that are the opposite of the sense that we are suggesting from our SDSS results. The resulting sSFR as a function of $\Sigma_{1\,{\rm kpc}}$ and $M_{\rm h}$ for central galaxies at $z = 0$ in GALICS is shown in Fig. 11(a).[4] $f_{\rm q}$ in this plane is similar. This combination of quenching produces strong vertical contours of sSFR above $M_{\rm crit}$ in contrast to what is observed in the SDSS (Fig. 2b).

Fig. 11(b) shows the prediction of the same model with the sense of the quenching reversed, i.e. accretion is halted and gas is removed from a galaxy when $B/T > 0.5$ while the $M_{\rm crit}$ criterion only cuts off accretion. The plot of $f_{\rm q}$ is similar. Note that this reversal of the quenching is the only change between the panels of Fig. 11. Qualitative agreement with the SDSS is vastly improved. Although quenching is slightly too strong at high $\Sigma_{1\,{\rm kpc}}$, the directions of the contours of sSFR are in rough agreement with the SDSS (vertical for low $\Sigma_{1\,{\rm kpc}}$ and roughly horizontal at mid-$\Sigma_{1\,{\rm kpc}}$). Given the large uncertainties of the model, the qualitative agreement with the SDSS after only one simple change is remarkable. These results show that two modes of quenching that effectively differ in duration can explain much of the quenching trends with $\Sigma_{1\,{\rm kpc}}$ and $M_{\rm h}$. They at least point the way for further study of quenching in SAMs, including experimenting with gas accretion and ejection with different criteria for halo- and compactness/bulge-quenching.

Thus, for central galaxies, galaxy compactness/bulges seems to play the role of the quick transition to quiescence while the halo plays the role of the slower fading of star formation. This is consistent with the two modes of quenching proposed in Barro et al. (2013) and Dekel & Burkert (2014) consisting of an early rapid quenching of compact star-forming galaxies and a later slower quenching of more diffuse galaxies. This is also consistent with the results and interpretation of Schawinski et al. (2014) who also suggest that quenching occurs in slow and fast modes. These authors show that early-type galaxies dominate the red sequence of galaxies whose

[4] We computed $\Sigma_{1\,{\rm kpc}}$ in GALICS by integrating the Hernquist (1990) profile for the bulge and starburst components and an exponential for the disc component out to 1 kpc. Galaxies for which $\Sigma_{1\,{\rm kpc}}$ is low despite having high B/T (a rarity in the SDSS) are removed to ensure that any quenching effect seen at low $\Sigma_{1\,{\rm kpc}}$ is due to the halo alone.

dust-corrected colour is largely unaffected by their halo mass. On the other hand, they show that the blue cloud and green valley are a continuous population of slowly evolving late-type galaxies whose colour is strongly reddened above $M_{\rm crit}$. The late-type galaxies above $M_{\rm crit}$ in their analysis are likely dominated by satellites (since they did not separate satellites from centrals), but we show explicitly in our analysis that quenching trends for central galaxies can be naturally explained if they experience both slow and fast modes of quenching.

5.3 Satellites

This picture may also explain the quenching behaviour of satellites. For these galaxies, groupcentric distance is roughly an indicator of how long they are influenced by their host halo. Since halo quenching is slower than $\Sigma_{1\,\rm kpc}$-related quenching, $f_{\rm q}$ and sSFR in the outer halo correlate with $\Sigma_{1\,\rm kpc}$ as they do for centrals and only weakly with the host $M_{\rm h}$. However, the influence of the halo here is non-negligible, and increases in importance towards the inner halo once the satellites have had enough time to be quenched by the halo. This effect is strongest for less massive satellites. By this time, $f_{\rm q}$ has reached 50 per cent for satellites in the inner regions of haloes of mass $3 \times 10^{12}\,{\rm M}_{\odot}$ ($\sim M_{\rm crit}$). Above $\sim 10^{13}\,{\rm M}_{\odot}$, these inner satellites are all quenched (Fig. 8). Some of these quenched galaxies were in fact quenched by $\Sigma_{1\,\rm kpc}$ before they arrived in the inner halo. These are the ones with high $\Sigma_{1\,\rm kpc}$, high M_* and low sSFR in the inner halo, and we suggest that this is why sSFR decreases with $\Sigma_{1\,\rm kpc}$ for quenched satellites here.

This interpretation is consistent with the findings of Muzzin et al. (2014) who study post-starburst satellites (i.e. those that were quenched quickly) and find that these quench around $0.5R_{200}$, i.e. the left-hand panels of Fig. 8. This picture is also consistent with findings of Wetzel et al. (2013) that satellite quenching time-scales are shorter at higher M_* but independent of $M_{\rm h}$, and with Wheeler et al. (2014) and Taranu et al. (2014) who find that low-mass satellites must have slow quenching time-scales, and at least slower than centrals (Tal et al. 2014).

Wetzel et al. (2013), Trinh et al. (2013) and Mok et al. (2013) proposed that satellite quenching is a 'delayed-then-rapid' process since neither rapid nor slow quenching adequately explains their observations. Instead, our framework suggests that the satellite population experiences a combination of slow and rapid quenching processes rather than a strictly chronological sequence. The quick process is the $\Sigma_{1\,\rm kpc}$-related quenching in the outskirts of haloes that also occurs in centrals, and the slower quenching is $M_{\rm h}$ related that is finally manifest once the satellite reaches the inner halo. Satellites at intermediate radii vary smoothly from one extreme to the other.

In addition, ram pressure stripping (a mechanism of halo quenching for satellites) strips only the gaseous halo of satellites at $\sim 1R_{\rm vir}$ from the halo centre. As a satellite migrates inward, ram pressure also strips cold gas, starting with the gas in the outer disc (Zinger et al., in preparation) which may lead to more rapid quenching.

6 CONCLUSION

In summary, our results include the following.

(i) Central stellar compactness strongly correlates with $f_{\rm q}$ for centrals at fixed $M_{\rm h}$, especially for mid-range values of $\Sigma_{1\,\rm kpc}$ ($\sim 10^{9\text{–}9.4}$). $M_{\rm h}$ correlates with sSFR (and $f_{\rm q}$ around $M_{\rm crit}$) at fixed $\Sigma_{1\,\rm kpc}$ for centrals with higher and lower $\Sigma_{1\,\rm kpc}$.

(ii) For central galaxies at fixed $M_{\rm h}$, the shape of the distribution of sSFR changes with $\Sigma_{1\,\rm kpc}$ such that galaxies with higher $\Sigma_{1\,\rm kpc}$ have a more numerous passive population. However at fixed $\Sigma_{1\,\rm kpc}$, increasing $M_{\rm h}$ shifts the entire distribution of sSFR to lower values without a significant change in shape. This is true at also fixed M_*. However, varying M_* at fixed $M_{\rm h}$ and $\Sigma_{1\,\rm kpc}$ does not change the sSFR distribution.

(iii) Most quenched centrals are both compact and live in massive haloes. However one in five quenched centrals above $M_{\rm h} = 10^{11.8}\,{\rm M}_{\odot}$ are diffuse ($\Sigma_{1\,\rm kpc} < 10^{9}\,{\rm M}_{\odot}\,{\rm kpc}^{-2}$). These may have been quenched by the halo alone, since they certainly did not quench through compaction-related processes.

(iv) $M_{\rm h}$-dependent quenching of satellites (at constant $\Sigma_{1\,\rm kpc}$) is seen most strongly in the inner regions of haloes. $f_{\rm q}$ and sSFR correlate strongly with $\Sigma_{1\,\rm kpc}$ and weakly with $M_{\rm h}$ in the outer regions of haloes. The correlation of quenching with $M_{\rm h}$ becomes stronger, especially for less massive satellites, towards the inner halo. Here, $f_{\rm q} \sim 0.5$ at $\sim M_{\rm crit}$, with satellites almost completely quenched in haloes $M_{\rm h} \gtrsim 10^{13}\,{\rm M}_{\odot}$. sSFR decreases with $\Sigma_{1\,\rm kpc}$ for these quenched satellites.

Our results suggest that both the halo and galaxy compactness play a role in the quenching of central and satellite galaxies. Galaxy inner compactness determines $f_{\rm q}$ while $M_{\rm h}$ determines sSFR for star-forming and quenched centrals, perhaps pointing to the quick and slower time-scales of bulge/compactness- and halo-related quenching as demonstrated in a SAM. For satellites, halo quenching becomes manifest once they have reached the inner halo, where nearly all are quenched above $M_{\rm crit}$. But along the way, compactness-related quenching operates on satellites independent of the halo.

ACKNOWLEDGEMENTS

We thank the anonymous referee for helpful comments that improved the paper. We acknowledge the helpful and stimulating discussions with Yuval Birnboim, Marcella Carollo, Will Hartley, Simon Lilly, Nir Mandelker, Kevin Schawinski, Benny Trakhtenbrot, Megan Urry and Andrew Wetzel. We thank Marcello Cacciato for kindly sharing his halo mass function code, and Andrea Cattaneo for assistance with the GALICS code. We also thank Frank van den Bosch and Xiaohu Yang for kindly providing the group catalogue for the SDSS DR7. This research has been partly supported at HU by ISF grant 24/12, by GIF grant G-1052-104.7/2009, by a DIP grant, by NSF grant AST-1010033 and by the I-CORE Program of the PBC and the ISF grant 1829/12. SMF and DCK acknowledge partial support for this work from an NSF grant AST 08-08133. Funding for the SDSS and SDSS-II has been provided by the Alfred P. Sloan Foundation, the Participating Institutions, the National Science Foundation, the U.S. Department of Energy, the National Aeronautics and Space Administration, the Japanese Monbukagakusho, the Max Planck Society, and the Higher Education Funding Council for England. The SDSS Web Site is http://www.sdss.org/. The SDSS is managed by the Astrophysical Research Consortium for the Participating Institutions. The Participating Institutions are the American Museum of Natural History, Astrophysical Institute Potsdam, University of Basel, University of Cambridge, Case Western Reserve University, University of Chicago, Drexel University, Fermilab, the Institute for Advanced Study, the Japan Participation Group, Johns Hopkins University, the Joint Institute for Nuclear Astrophysics, the Kavli Institute for Particle Astrophysics and Cosmology, the Korean Scientist Group, the Chinese Academy of Sciences (LAMOST), Los Alamos National Laboratory, the Max-Planck-Institute for

Astronomy (MPIA), the Max-Planck-Institute for Astrophysics (MPA), New Mexico State University, Ohio State University, University of Pittsburgh, University of Portsmouth, Princeton University, the United States Naval Observatory, and the University of Washington.

REFERENCES

Abadi M. G., Moore B., Bower R. G., 1999, MNRAS, 308, 947
Abazajian K. N. et al., 2009, ApJS, 182, 543
Adelman-McCarthy J. K. et al., 2008, ApJS, 175, 297
Baldry I. K., Glazebrook K., Brinkmann J., Ivezić Ž., Lupton R. H., Nichol R. C., Szalay A. S., 2004, ApJ, 600, 681
Baldry I. K., Balogh M. L., Bower R. G., Glazebrook K., Nichol R. C., Bamford S. P., Budavari T., 2006, MNRAS, 373, 469
Balogh M. L., Navarro J. F., Morris S. L., 2000, ApJ, 540, 113
Balogh M. L., Baldry I. K., Nichol R., Miller C., Bower R., Glazebrook K., 2004, ApJ, 615, L101
Bamford S. P. et al., 2009, MNRAS, 393, 1324
Barro G. et al., 2013, ApJ, 765, 104
Bell E. F., 2008, ApJ, 682, 355
Bell E. F., McIntosh D. H., Katz N., Weinberg M. D., 2003, ApJS, 149, 289
Bell E. F. et al., 2012, ApJ, 753, 167
Bigiel F. et al., 2011, ApJ, 730, L13
Birnboim Y., Dekel A., 2003, MNRAS, 345, 349
Birnboim Y., Dekel A., Neistein E., 2007, MNRAS, 380, 339
Blanton M. R., Roweis S., 2007, AJ, 133, 734
Blanton M. R. et al., 2003, AJ, 125, 2348
Blanton M. R., Eisenstein D., Hogg D. W., Schlegel D. J., Brinkmann J., 2005a, ApJ, 629, 143
Blanton M. R. et al., 2005b, AJ, 129, 2562
Bluck A. F. L., Mendel J. T., Ellison S. L., Moreno J., Simard L., Patton D. R., Starkenburg E., 2014, MNRAS, 441, 599
Bournaud F., Elmegreen B. G., Elmegreen D. M., 2007, ApJ, 670, 237
Bower R. G., Benson A. J., Malbon R., Helly J. C., Frenk C. S., Baugh C. M., Cole S., Lacey C. G., 2006, MNRAS, 370, 645
Brinchmann J., Charlot S., White S. D. M., Tremonti C., Kauffmann G., Heckman T., Brinkmann J., 2004, MNRAS, 351, 1151
Bruce V. A. et al., 2012, MNRAS, 427, 1666
Bruce V. A. et al., 2014, MNRAS, 444, 1001
Bundy K. et al., 2006, ApJ, 651, 120
Bundy K. et al., 2010, ApJ, 719, 1969
Carollo C. M. et al., 2013, ApJ, 776, 71
Carollo C. M. et al., 2014, preprint (arXiv:1402.1172)
Cattaneo A. et al., 2007, MNRAS, 377, 63
Cattaneo A., Dekel A., Faber S. M., Guiderdoni B., 2008, MNRAS, 389, 567
Cattaneo A., Woo J., Dekel A., Faber S. M., 2013, MNRAS, 430, 686
Cheung E. et al., 2012, ApJ, 760, 131
Cibinel A. et al., 2013, ApJ, 776, 72
Coil A. L., Weiner B. J., Holz D. E., Cooper M. C., Yan R., Aird J., 2011, ApJ, 743, 46
Cooper M. C. et al., 2008, MNRAS, 383, 1058
Croton D. J. et al., 2006, MNRAS, 365, 11
Dekel A., Birnboim Y., 2006, MNRAS, 368, 2
Dekel A., Burkert A., 2014, MNRAS, 438, 1870
Dekel A., Krumholz M. R., 2013, MNRAS, 432, 455
Dekel A., Mandelker N., 2014, MNRAS, 444, 2071
Dekel A., Sari R., Ceverino D., 2009, ApJ, 703, 785
Doi M. et al., 2010, AJ, 139, 1628
Eisenstein D. J., Hu W., 1998, ApJ, 496, 605
Fan X. et al., 2001, AJ, 122, 2833
Fang J. J., Faber S. M., Koo D. C., Dekel A., 2013, ApJ, 776, 63
Franx M., van Dokkum P. G., Schreiber N. M. F., Wuyts S., Labbé I., Toft S., 2008, ApJ, 688, 770
Gabor J. M., Davé R., 2014, MNRAS, 447, 374
Gao Y., Solomon P. M., 2004, ApJ, 606, 271
Gómez P. L. et al., 2003, ApJ, 584, 210
Goto T., Yamauchi C., Fujita Y., Okamura S., Sekiguchi M., Smail I., Bernardi M., Gomez P. L., 2003, MNRAS, 346, 601
Gunn J. E., Gott J. R., III, 1972, ApJ, 176, 1
Gunn J. E. et al., 1998, AJ, 116, 3040
Gunn J. E. et al., 2006, AJ, 131, 2332
Haas M. R., Schaye J., Jeeson-Daniel A., 2012, MNRAS, 419, 2133
Haines C. P., Gargiulo A., La Barbera F., Mercurio A., Merluzzi P., Busarello G., 2007, MNRAS, 381, 7
Hansen S. M., Sheldon E. S., Wechsler R. H., Koester B. P., 2009, ApJ, 699, 1333
Hartley W. G. et al., 2013, MNRAS, 431, 3045
Hartley W. G., Conselice C. J., Mortlock A., Foucaud S., Simpson C., 2014, preprint (arXiv:1406.6058)
Hatton S., Devriendt J. E. G., Ninin S., Bouchet F. R., Guiderdoni B., Vibert D., 2003, MNRAS, 343, 75
Hernquist L., 1990, ApJ, 356, 359
Hogg D. W. et al., 2003, ApJ, 585, L5
Hopkins P. F. et al., 2009, MNRAS, 397, 802
Hopkins P. F. et al., 2010, ApJ, 724, 915
Kauffmann G. et al., 2003a, MNRAS, 341, 33
Kauffmann G. et al., 2003b, MNRAS, 341, 54
Kauffmann G., White S. D. M., Heckman T. M., Ménard B., Brinchmann J., Charlot S., Tremonti C., Brinkmann J., 2004, MNRAS, 353, 713
Kennicutt R. C., Jr, 1989, ApJ, 344, 685
Kennicutt R. C., Jr, 1998, ApJ, 498, 541
Kereš D., Katz N., Weinberg D. H., Davé R., 2005, MNRAS, 363, 2
Kereš D., Katz N., Fardal M., Davé R., Weinberg D. H., 2009, MNRAS, 395, 160
Knobel C. et al., 2013, ApJ, 769, 24
Knobel C., Lilly S. J., Woo J., Kovac K., 2014, preprint (arXiv:1408.2553)
Kodama T., Balogh M. L., Smail I., Bower R. G., Nakata F., 2004, MNRAS, 354, 1103
Koopmann R. A., Kenney J. D. P., 1998, ApJ, 497, L75
Kormendy J., Ho L. C., 2013, ARA&A, 51, 511
Kovač K. et al., 2014, MNRAS, 438, 717
Kroupa P., 2001, MNRAS, 322, 231
Lang P. et al., 2014, ApJ, 788, 11
Larson R. B., Tinsley B. M., Caldwell C. N., 1980, ApJ, 237, 692
Lotz J. M., Jonsson P., Cox T. J., Croton D., Primack J. R., Somerville R. S., Stewart K., 2011, ApJ, 742, 103
McGrath E. J., Stockton A., Canalizo G., Iye M., Maihara T., 2008, ApJ, 682, 303
Mandelker N., Dekel A., Ceverino D., Tweed D., Moody C. E., Primack J., 2014, MNRAS, 443, 3675
Martig M., Bournaud F., Teyssier R., Dekel A., 2009, ApJ, 707, 250
Mendel J. T., Simard L., Ellison S. L., Patton D. R., 2013, MNRAS, 429, 2212
Mihos J. C., Hernquist L., 1994, ApJ, 437, L47
Mok A. et al., 2013, MNRAS, 431, 1090
Moore B., Lake G., Katz N., 1998, ApJ, 495, 139
Moster B. P., Somerville R. S., Maulbetsch C., van den Bosch F. C., Macciò A. V., Naab T., Oser L., 2010, ApJ, 710, 903
Muzzin A. et al., 2014, ApJ, 796, 65
Navarro J. F., Frenk C. S., White S. D. M., 1997, ApJ, 490, 493
Noguchi M., 1999, ApJ, 514, 77
Ocvirk P., Pichon C., Teyssier R., 2008, MNRAS, 390, 1326
Omand C. M. B., Balogh M. L., Poggianti B. M., 2014, MNRAS
Padmanabhan N. et al., 2008, ApJ, 674, 1217
Peng Y. et al., 2010, ApJ, 721, 193
Peng Y.-j., Lilly S. J., Renzini A., Carollo M., 2012, ApJ, 757, 4
Pflamm-Altenburg J., Kroupa P., 2009, ApJ, 706, 516
Quadri R. F., Williams R. J., Franx M., Hildebrandt H., 2012, ApJ, 744, 88
Read J. I., Wilkinson M. I., Evans N. W., Gilmore G., Kleyna J. T., 2006, MNRAS, 366, 429

Rees M. J., Ostriker J. P., 1977, MNRAS, 179, 541
Rines K., Geller M. J., Kurtz M. J., Diaferio A., 2005, AJ, 130, 1482
Robaina A. R., Hoyle B., Gallazzi A., Jiménez R., van der Wel A., Verde L., 2012, MNRAS, 427, 3006
Saintonge A. et al., 2011, MNRAS, 415, 61
Salim S. et al., 2007, ApJS, 173, 267
Salim S., Fang J. J., Rich R. M., Faber S. M., Thilker D. A., 2012, ApJ, 755, 105
Sanders D. B., Mirabel I. F., 1996, ARA&A, 34, 749
Sanders D. B., Scoville N. Z., Soifer B. T., 1991, ApJ, 370, 158
Schawinski K. et al., 2014, MNRAS, 440, 889
Skibba R. A., Sheth R. K., 2009, MNRAS, 392, 1080
Stockton A., Canalizo G., Maihara T., 2004, ApJ, 605, 37
Stoughton C. et al., 2002, AJ, 123, 485
Strateva I. et al., 2001, AJ, 122, 1861
Szomoru D., Franx M., van Dokkum P. G., 2012, ApJ, 749, 121
Tal T. et al., 2014, ApJ, 789, 164
Tanaka M., Goto T., Okamura S., Shimasaku K., Brinkmann J., 2004, AJ, 128, 2677
Taranu D. S., Hudson M. J., Balogh M. L., Smith R. J., Power C., Oman K. A., Krane B., 2014, MNRAS, 440, 1934
Tinker J., Kravtsov A. V., Klypin A., Abazajian K., Warren M., Yepes G., Gottlöber S., Holz D. E., 2008, ApJ, 688, 709
Toomre A., Toomre J., 1972, ApJ, 178, 623
Trinh C. Q., Barton E. J., Bullock J. S., Cooper M. C., Zentner A. R., Wechsler R. H., 2013, MNRAS, 436, 635
van den Bergh S., 2009, ApJ, 702, 1502
van den Bosch F. C., Pasquali A., Yang X., Mo H. J., Weinmann S., McIntosh D. H., Aquino D., 2008, preprint (arXiv:0805.0002)
van der Wel A. et al., 2011, ApJ, 730, 38
van de Voort F., Schaye J., Booth C. M., Haas M. R., Dalla Vecchia C., 2011, MNRAS, 414, 2458
van Dokkum P. G. et al., 2008, ApJ, 677, L5
van Dokkum P. G. et al., 2011, ApJ, 743, L15
Villalobos Á., De Lucia G., Borgani S., Murante G., 2012, MNRAS, 424, 2401
Vogt N. P., Haynes M. P., Giovanelli R., Herter T., 2004, AJ, 127, 3300
von der Linden A., Wild V., Kauffmann G., White S. D. M., Weinmann S., 2010, MNRAS, 404, 1231
Weinmann S. M., van den Bosch F. C., Yang X., Mo H. J., 2006, MNRAS, 366, 2
Wetzel A. R., Tinker J. L., Conroy C., 2012, MNRAS, 424, 232
Wetzel A. R., Tinker J. L., Conroy C., van den Bosch F. C., 2013, MNRAS, 432, 336
Wheeler C., Phillips J. I., Cooper M. C., Boylan-Kolchin M., Bullock J. S., 2014, MNRAS, 442, 1396
Wilman D. J., Zibetti S., Budavári T., 2010, MNRAS, 406, 1701
Wolf C. et al., 2009, MNRAS, 393, 1302
Woo J. et al., 2013, MNRAS, 428, 3306
Wuyts S. et al., 2011, ApJ, 742, 96
Wuyts S. et al., 2012, ApJ, 753, 114
Yang X., Mo H. J., van den Bosch F. C., Pasquali A., Li C., Barden M., 2007, ApJ, 671, 153
Yang X., Mo H. J., van den Bosch F. C., Zhang Y., Han J., 2012, ApJ, 752, 41
Yesuf H. M., Faber S. M., Trump J. R., Koo D. C., Fang J. J., Liu F. S., Wild V., Hayward C. C., 2014, ApJ, 792, 84
York D. G. et al., 2000, AJ, 120, 1579
Young J. S., Schloerb F. P., Kenney J. D., Lord S. D., 1986, ApJ, 304, 443
Zolotov A., Dekel A., Mandelker N., Tweed D., Inoue S., DeGraf C., Ceverino D., Primack J., 2014, in press

This paper has been typeset from a TEX/LATEX file prepared by the author.